

Coversheet

Dissolution methods for strontium isotope stratigraphy: Guidelines for the use of argillaceous, dolomitic limestone

Xi Chen ^a, Ying Zhou ^a

^aDepartment of Earth Sciences, University College London, Gower Street, London, WC1E 6BT, UK

Email Addresses: helen.xi.chen.19@ucl.ac.uk (Xi Chen), y-zhou@ucl.ac.uk (Ying Zhou)

This manuscript has been submitted for publication in Chemical Geology. Please note that this paper is a non-peer reviewed EarthArXiv preprint. Subsequent version of this manuscript may have slightly different content. If accepted, the final version of this manuscript will be available via the “Peer-reviewed Publication DOI” link on the right-hand side of this webpage. Please feel free to contact any of the authors; we welcome feedback.

1 **Dissolution methods for strontium isotope stratigraphy: Guidelines for the**
2 **use of argillaceous, dolomitic limestone**

3 Xi Chen ^a, Ying Zhou ^a

4 ^aDepartment of Earth Sciences, University College London, Gower Street, London, WC1E 6BT, UK

5 Email Addresses: helen.xi.chen.19@ucl.ac.uk (Xi Chen), y-zhou@ucl.ac.uk (Ying Zhou)

6 **Abstract**

7 In recent years, various sample preparation methods have been developed to
8 extract a primary Sr isotope signal from carbonate rocks. However, there has been
9 little consensus around the best method due to natural variability in sample purity and
10 mineralogy. For this study, we conducted systematic leaching experiments, focussing
11 mainly on generally less favoured argillaceous and dolomitic limestones, using
12 samples from the Mesoproterozoic Gaoyuzhuang Formation. Learning from previous
13 studies, a multistep leaching approach was used to explore strontium isotope leaching
14 systematics and extract near-primary isotopic ratios. For argillaceous and dolomitic
15 limestone, the first 10%-30% dilute acetic acid leach, following an ammonium acetate
16 (NH₄Ac) prewash, yielded the lowest, demonstrably least altered seawater ⁸⁷Sr/⁸⁶Sr
17 ratios. Subsequent dissolution steps exhibited significantly elevated ⁸⁷Sr/⁸⁶Sr, Rb/Sr,
18 Al/Ca, and Mg/Ca ratios, indicating greater contributions from aluminosilicates and
19 dolomite in the leachates. Lanthanide rare earth element and yttrium (REY)
20 concentrations were also examined for each leaching step. In most cases, seawater-
21 like REY patterns with the highest Y/Ho ratios (mostly > 36) occur in the first
22 leaching step after ammonium acetate prewash, which is consistent with the Sr isotope
23 study. However, one organic-rich sample (TOC_{total} ~1.3%) with a near-seawater Sr
24 isotope value exhibits a non-seawater-like REY pattern, possibly indicating that early
25 diagenetic exchange during organic remineralization may influence the REY pattern

26 of carbonate rocks without necessarily changing Sr isotopes. We applied previously
27 proposed leaching cut-offs (preleach 30% ~ 40%, 60% ~ 70%), alongside the cut-off
28 proposed from this study, for samples with various Mg/Ca and carbonate purities. We
29 found that for the same argillaceous and dolomitic carbonate rocks, applying higher
30 leaching cut-offs might cause sizeable error compared with targeting the first 10% ~
31 30% directly after NH₄Ac prewash. However, no significant differences were evident
32 for high purity, and low Mg/Ca limestones, highlighting the importance of matching
33 different sample types to the most appropriate dissolution method. Here we
34 demonstrate that argillaceous, even partially dolomitized limestones could help fill
35 gaps in the Precambrian seawater Sr isotope curve, especially where higher purity
36 limestone successions are not readily available.

37 **Key Words**

38 Dissolution methods; strontium isotopes; argillaceous limestone; dolomitic
39 limestone

40 **1. Introduction**

41 The secular trend of seawater strontium isotope ratio ($^{87}\text{Sr}/^{86}\text{Sr}$) reflects variations
42 in the relative contributions of continental versus mantle reservoirs to ocean
43 composition (Spooner, 1976; Veizer, 1989). The ocean residence time of Sr is much
44 longer than the ocean circulation time ($\sim 10^6$ vs. $\sim 10^3$ years, respectively), and so
45 strontium isotopes are believed to be homogeneously distributed in seawater at any
46 given time (Broecker and Peng, 1983; Elderfield, 1986; Hodell et al., 1990). As a
47 consequence, strontium isotope stratigraphy (SIS) has been widely used for
48 chemostratigraphic correlation (Burke et al., 1982; Elderfield, 1986; McArthur, 1994;
49 Veizer et al., 1999); dating by comparison to standard reference curves (McArthur et
50 al., 2012, 2020); tracing diagenetic processes and depositional environment
51 (Kuznetsov et al., 2010; Stüeken et al., 2017); and testing hypotheses of tectonic,
52 biological and climatic evolution on geological timescales (e.g., Halverson, 2007;
53 Shields, 2007; Hawkesworth et al., 2016; Cawood et al., 2018).

54 SIS studies must rely on diagenetically well-preserved chemical precipitates and
55 well-honed dissolution methods. Diagenetic processes tend to increase $^{87}\text{Sr}/^{86}\text{Sr}$
56 values when interstitial fluids are influenced by evolved K-bearing silicates (e.g.,
57 Shields and Veizer, 2002; Fairchild et al., 2018), or decrease Sr isotope composition
58 when diagenetic fluids are influenced by mafic components, hydrothermal fluids or
59 pressure solution of older, underlying carbonate rocks (e.g., Miller et al., 2008; Brand
60 et al., 2010; Satkoski et al., 2017; Cui et al., 2020). Unfortunately, the well preserved,
61 low-Mg calcite fossils, widely used in Phanerozoic SIS studies, are not available in
62 Precambrian rocks, and so fine-grained carbonate components (e.g., diagenetic calcite
63 microspar cement; Zhou et al., 2020), bulk carbonate rocks (e.g., micrite; Bailey et al.,
64 2000) or non-carbonate rocks such as barite (e.g., McCulloch, 1994; Satkoski et al.,

65 2016; Roerdink et al., 2022), gypsum or anhydrite (e.g., Kah et al., 2001) and
66 francolite (Li et al., 2011) have all been used instead for this purpose. Apart from
67 diagenetic alteration, the leaching of detrital aluminosilicate phases during sample
68 preparation can also introduce unintended Sr contamination, which is either released
69 by ion exchange during the initial leaching stage or aluminosilicate dissolution during
70 the later leaching process (McArthur, 1994; Bailey et al., 2000; Bellefroid et al.,
71 2018). Clay contamination during sample preparation normally would lead to Sr
72 isotopes much higher than expected (Bailey et al., 2000), may result in overcorrection
73 for radioactive Rb decay (Shields and Veizer, 2002), and can mask the original
74 diagenetic trend in a suite of samples (Bellefroid et al., 2018). Therefore, when
75 conducting SIS, it is crucial that Sr is isolated from targeted and least altered minerals
76 without contamination from extraneous phases, which requires appropriate dissolution
77 methods.

78 The dissolution methods used in SIS studies can be divided into three main types:
79 single-step bulk leaching methods, two-step sequential leaching methods and
80 multiple-step sequential leaching methods (see recent review by Chen et al., 2022 and
81 references therein). The most commonly used and effective sequential leaching
82 method uses dilute acetic acid to target a certain proportion of pure carbonate,
83 following an initial pre-leach with ammonium acetate or acetic acid to remove
84 exchangeable Rb and Sr, while aiming to leave at least 10% carbonate undissolved
85 (Bailey et al., 2000). This method has been developed further and is now widely used
86 to extract primary carbonate signals from different types of carbonate rocks, using
87 various pre-leaching cut-offs. For example, Bailey et al. (2000), confirmed
88 subsequently by Li et al., (2011), suggested dissolving 30% ~ 40% of the carbonate
89 portion of a sample, before targeting the following 30% ~ 40% for isotopic analysis.

90 Liu et al., (2013) suggested to pre-leach up to 70% ~ 80% of a dolostone sample,
91 targeting the next 10% ~ 20% for analysis. Finally, Li et al., (2020) suggested an
92 acidic pre-leach to dissolve ~60% of the carbonate, before targeting the next ~20% for
93 both limestone and dolostone samples, but with emphasis on sample purity > 75%
94 and > 90% for limestone and dolostone, respectively.

95 From the above, it is evident that few of any studies have sought to improve Sr
96 isotope leaching methods for low purity and/or partially dolomitised samples, despite
97 the lack of high purity limestones and large data gaps in Precambrian successions
98 (Shields and Veizer, 2002; Chen et al., 2022). Moreover, without a clear
99 definition/classification system for sample purity and sample types, the application
100 thresholds between different methods remain ill-defined, with little consensus as to
101 the most appropriate method. Therefore, it is imperative to conduct a systematic
102 methodological study on the abundant but less favoured argillaceous (often referred to
103 as ‘dirty’ or ‘muddy’) and/or dolomitic limestones, and also test different leaching
104 cut-offs / methods for samples using clear purity and Mg/Ca classification.

105 The rare earth element (REE) plus yttrium (REY) compositions of marine
106 carbonate rocks could reveal depositional environment, redox conditions and
107 diagenetic alteration (e.g., Satkoski et al., 2017; Verdel et al., 2018), thus might help
108 us to determine if the Sr isotope data record seawater signal. The typical seawater
109 REY profile shows progressive enrichment in heavier REE (James et al., 1995), while
110 REY carbonate systematics are relatively resistant to diagenetic exchange compared
111 with Sr isotopes due to the high partition coefficients of REY between calcite and
112 seawater and generally low REY concentrations in diagenetic fluids (Zhong and
113 Mucci, 1995; Webb and Kamber, 2000). However, carbonate REY components are
114 very sensitive to detrital contamination due to the much higher REY contents and

115 distinctly different shale - normalized REE patterns in detrital minerals (e.g.,
116 Nothdurft et al., 2004). Such a high sensitivity for clay contamination is also expected
117 for Sr isotopes, and so comparing the REY pattern and Sr isotope ratios of individual
118 leaching steps could help to validate the leaching method, especially for low purity
119 carbonate rocks (James et al., 1995). The relatively clean proportion of the
120 argillaceous and dolomitic carbonates during leaching procedures might be expected
121 to demonstrate the most pristine, 'marine' REY patterns and Sr isotope values.

122 Based on earlier studies, such as Chilingar, (1957) and Zhou et al., (2020), we
123 divided samples into four types according to their Mg/Ca weight ratios, which are
124 limestone (LST, Mg/Ca < 0.025), slightly dolomitic limestone (SDL, 0.025 < Mg/Ca
125 < 0.25), highly dolomitic limestone (HDL, 0.25 < Mg/Ca < 0.6) and dolostone (DST,
126 Mg/Ca > 0.6). We define sample purity < 80% as argillaceous/low purity samples,
127 and sample purity > 80% as relatively pure samples. In this study, we mainly aim to
128 1) conduct a systematic method study focusing mainly on argillaceous and dolomitic
129 limestones (sample purity < 80%, 0.025 < Mg/Ca < 0.6); 2) use REY patterns to assist
130 in the discussion of Sr isotope leaching results and explore the connections and
131 differences between these two systems; 3) explore the fitness of different methods for
132 different types of rock by applying previously published, commonly used leaching
133 cut-offs to samples with various purities and Mg/Ca ratios; and 4) propose new
134 thresholds for sample screening in future SIS studies.

135 **2. Geological setting and sample descriptions**

136 **2.1. Geological background**

137 The ~1.65-1.4 Ga Jixian Group consists of five formations (Gaoyuzhuang,
138 Yangzhuang, Wumishan, Hongshuizhuang, and Tieling in ascending order), which
139 represent near-continuous marine deposition within the Yanliao Basin, North China
140 Craton. The ~1.6-1.55 Ga Gaoyuzhuang Formation is further divided into four
141 lithological members in ascending order: Guandi Member (M1), Sangshu'an Member
142 (M2), Zhangjiayu Member (M3) and Huanxiusi Member (M4). Most samples in this
143 study were collected from the ~1.57-1.56 Ga Zhangjiayu Member (M3) (Li et al.,
144 2010; Tian et al., 2015), through an interval that covers a negative carbon isotope
145 excursion (Li et al., 2003; Guo et al., 2013; Zhang et al., 2018). The Zhangjiayu
146 Member consists mainly of limestone and dolomitic limestone deposited in the
147 shallow marine environment, with argillaceous and variably dolomitised limestone
148 and black shale mainly in the lower part, showing a shallowing-upward cycle (e.g.,
149 Mei et al., 2005; Zhang et al., 2018). The impure, dolomitic limestones of Zhangjiayu
150 Member provide a good opportunity for us to examine the leaching method for this
151 type of rock. Based on a new compilation of the Precambrian seawater Sr isotope
152 curve (Chen et al., 2022), the published and screened seawater $^{87}\text{Sr}/^{86}\text{Sr}$ data between
153 1.60 Ga and 1.55 Ga range from ~0.7046 to ~0.7056 (e.g., Ray et al., 2003;
154 Kuznetsov et al., 2008; Bellefroid et al., 2018; Tan et al., 2020), which are compared
155 with data obtained in this study.

156 **2.2. Samples**

157 Samples of varying purity and dolomitization were collected from the Zhangjiayu
158 Member (M3) at Jixian (J), Pingquan (P), Gangou (G), Kuancheng (K), Huanxiusi

159 (HXSZ) and Sangshu'an (SSAZ) sections, and underlying Huanxiusi Member (M4,
160 abbreviated to HXS) on the North China Craton. Samples analyzed in this study were
161 micro-drilled to extract powder to avoid visibly secondary portions such as cross-
162 cutting veins, late-stage void filling spar and dissolution features etc. After that,
163 powders of each sample were dissolved in 2% HNO₃ for bulk carbonate major and
164 trace elements before undergoing leaching steps. Stable isotopes ($\delta^{13}\text{C}$ and $\delta^{18}\text{O}$) were
165 also analyzed to help with sample selection and diagenetic screening. Five samples
166 (J95, G99, K46, G90, HXSZ4) from four different sections (Jixian, Gangou,
167 Kuancheng and Huanxiusi) of Zhangjiayu Member (M3) were selected to develop a
168 leaching method for argillaceous and dolomitic limestone. These samples have Mg/Ca
169 ratios ranging from ~0.06 to 0.4 with carbonate contents ranging from 50% to 75%,
170 and with few obvious signs of significant diagenetic alteration (e.g., in most cases
171 Mn/Sr <1, $\delta^{13}\text{C}$ close to ~0, $\delta^{18}\text{O}$ at -3 ~ -5‰). The five samples were used for
172 sequential leaching experiments alongside rock standard LS19 (a pure limestone from
173 the Huaibei group, Mg/Ca = 0.02) from Zhou et al., (2020) with a published Sr
174 isotope value of 0.705439 (± 3); and one reference material CRM 88a (a pure
175 dolostone, Mg/Ca = 0.6) with a published Sr isotope value of 0.71022 (Stammeier et
176 al., 2020). The detailed bulk rock information for all samples used for this study is
177 summarized in **Table 1**. Another twenty samples with various sample purities and
178 Mg/Ca ratios were studied to examine the leaching methods, the bulk carbonate
179 information of which is reported alongside Sr isotope result in **Table 4** in section 4.3.

Sample Labels	Sample types	Carbonate content (%)	Mg/Ca (g/g)	Mn/Sr (g/g)	Rb/Sr (mg/g)	K/Ca (mg/g)	Al/Ca (mg/g)	Ba/Ca (mg/g)	Fe/Ca (mg/g)	[Sr/Ca+Mg] (ppm)	$\delta^{13}\text{C}_{\text{VPDB}}$ (‰)	$\delta^{18}\text{O}_{\text{VPDB}}$ (‰)	Age (Ga)
LS19	LST	90%	0.02	0.03	0.1	0.38	0.39	0.01	0.10	988			~0.96
J95	SDL	70%	0.06	0.14	5.48	0.79	2.15	0.06	2.02	672	-0.64	-5.25	~1.56-1.57
G99	SDL	57%	0.11	0.51	36.90	4.75	5.73	0.19	17.84	876	-1.27	-4.89	~1.56-1.57
K46	SDL	75%	0.20	0.34	11.47	1.73	3.43	0.09	5.91	661	-0.59	-4.52	~1.56-1.57
G90	HDL	62%	0.40	1.31	30.67	2.01	2.80	0.09	14.12	368	-0.99	-3.49	~1.56-1.57
HXSZ4	HDL	62%	0.30	0.28	6.88	1.28	2.46	0.11	6.89	519	-0.52	-4.21	~1.56-1.57
88a	DST	98%	0.6	4.83	3.02	4.60	4.00	0.01	9.00	121			

Table 1. Bulk carbonate information for samples used for step-leaching experiments.

180 **3. Methods**

181 **3.1. Sequential leaching procedure**

182 3.1.1. Ten-step sequential leaching procedure

183 Micro-drilled sample powder was ground by hand using an agate pestle and
184 mortar to avoid coarse flakes, and then around 100-200 mg of each sample was
185 transferred to 10 ml centrifuge tubes to carry out the sequential leaching procedure.
186 Modified after Bailey et al., (2000), a ten-step leaching procedure was applied to
187 argillaceous, dolomitic limestones (J95, G99, K46, G90, HXSZ4) and CRM 88a,
188 while a six-step leaching procedure was applied to pure limestone LS19. All samples
189 have been prewashed with 1M ammonium acetate, followed by dilute acetic acid
190 (0.05 M-0.5 M) dissolution. In each step, based on total carbonate content, the acid
191 volumes were designed to dissolve ~10% carbonate for argillaceous and dolomitic
192 limestones and CRM 88a, and ~20% for pure limestone LS19. After the acid was
193 added, samples were ultrasonically agitated (0.5 hr-2 hr) and allowed to stand for 0.5
194 hr-2 hr at 25-40°C, then were centrifuged at 3600 rpm for 5mins. The supernatant was
195 collected for Sr isotope and elemental analysis, and the residue washed with ultrapure
196 water one time before the next leaching step. The carbonate proportion being leached
197 out in each step was calculated by using mass of (CaCO₃+MgCO₃) in each leaching
198 step divided by mass of (CaCO₃+MgCO₃) in the whole sample. In total, more than
199 95% of carbonate was dissolved from each sample. Detailed leaching protocol is
200 summarized in **Table 2**.

Steps	LST	SDL	HDL	DST	Reaction time
S0	5 ml 1 M NH ₄ HAc	30 mins usb at room temperature			
S1-S2	7.5 ml 0.05 M HAc	4 ml 0.2 M HAc	2.5 ml 0.5 M HAc	5 ml 0.5 M HAc	30 mins usb + 30 mins stand at room temperature
S3-S5	7.5 ml 0.05 M HAc	5 ml 0.2 M HAc	3.5 ml 0.5 M HAc	8 ml 0.5 M HAc	30 mins -1 hr usb + 30 mins -1 hr stand at room temperature
S6-S8		8 ml 0.2 M HAc	6 ml 0.5 M HAc	10 ml 0.5 M HAc	2 hr usb + 2 hr stand at 30-40°C
S9		10 ml 0.5 M HAc	10 ml 0.5 M HAc	10 ml 0.5 M HAc	Overnight on mixing roller at room temperature

Table 2. Sequential leaching protocol. 6-step leaching (design to dissolve 20% carbonate in each step) was conducted for pure limestone (LST); and 10-step leaching (designed to dissolve 10% carbonate in each step) was conducted for SDL, HDL, DST. *pH* of each reagent: 1 M NH₄HAc (~7); 0.05 M HAc (~3); 0.2 M HAc (~2.7); 0.5 M HAc (~2.5). usb: ultrasonic bath.

201 3.1.2. Leaching methods' comparison

202 Twenty samples with various sample purities and Mg/Ca from 0 to 0.6 (i.e.,
203 limestone, slightly, and highly dolomitic limestone) from Gaoyuzhuang Formation
204 were selected to examine the suitability of various leaching cut-offs for different types
205 of rocks (note: samples with Mg/Ca > 0.6 are not examined in this study). The
206 following leaching methods are compared: *method 1* - prewash using ammonium
207 acetate, then target the first 10% ~ 30% (this study); *method 2* - preleach 30% ~ 40%,
208 then target the next 30% ~ 40% (Bailey et al., 2000; Li et al., 2011); *method 3* -
209 preleach 60% ~ 70%, then target the next ~ 20% (Liu et al., 2013; Li et al., 2020). We
210 conducted a four-step leaching experiment (simplified from the ten-step leaching
211 method above), which was designed to dissolve ~30% carbonate in each step after a 1
212 M ammonium acetate prewash. Accordingly, the leachates from steps 1, 2 and 3
213 roughly correspond to cut-offs in methods 1, 2, and 3 respectively, which were then
214 measured for Sr isotopes.

215 3.2. Elemental analyses

216 Elemental analyses, including major, trace elements and REY analysis, were
217 carried out in the Cross-Faculty Elemental Analysis Facility, University College
218 London (UCL), for solutions of bulk carbonate and all leaching supernatants of
219 selected samples and rock standards. For bulk carbonate measurement, sample
220 powder (~10-20 mg) was dissolved in 5ml 2% HNO₃ for 24 hr, then centrifuged at
221 3600 rpm, for 5mins. The supernatant was collected and diluted with 2% HNO₃ for
222 elemental analysis. Major elements including Ca, Mg, K, Na, Fe, Mn, Al, and Sr were
223 measured by inductively coupled plasma optical emission spectrometry (Varian 720
224 ICP-AES). The analyses achieved an error of < 3 % for the analyzed elements based

225 on long-term reproducibility of the laboratory measurement. Trace element Rb, Y and
226 rare earth element (REE) concentrations of carbonate leachates were analysed by
227 inductively coupled plasma mass spectrometry (Agilent 7900 ICP-MS) and run
228 against multi-element matrix-matched standards within an appropriate concentration
229 range. Replicate extractions gave a relative standard deviation (RSD) of less than 5%.
230 The stepwise REY concentration is calculated based on the mass of Ca, Mg carbonate
231 being leached out (i.e., mass of REY divided by mass of $\text{CaCO}_3 + \text{MgCO}_3$ in each
232 step). All REY concentrations were normalized to post-Archean Australian Shale
233 (PAAS: Pourmand et al., 2012).

234 3.3. Sr, C, O isotope analysis

235 For Sr isotopes, small polypropylene columns with polypropylene frits ($\sim 30\mu\text{m}$)
236 and $\sim 1\text{cm}$ thickness of Eichrom® Sr specific resin were used for Sr separation in an
237 ISO 7 (Class 10000) geochemistry laboratory at UCL. The supernatant in each
238 leaching step was dried in Teflon beakers on a hotplate before being dissolved in
239 0.5ml 4M nitric acid and then passed through the precleaned and conditioned
240 columns. The collected eluant was then dried and redissolved in 2% HNO_3 for Sr
241 isotope measurement. The $^{87}\text{Sr}/^{86}\text{Sr}$ ratios were measured using a Nu Instruments
242 Plasma 3 multi-collector inductively coupled plasma mass spectrometer (MC-ICP-
243 MS) at UCL. Each sample was bracketed by two measurements of NBS 987.
244 Systematic offsets in analytical sessions were corrected by normalizing the average of
245 the bracketing standards to a reference value (NBS 987) of $^{87}\text{Sr}/^{86}\text{Sr} = 0.710252$. The
246 internal standard error (2se) for each sample and standard deviation (2sd) for repeated
247 measurements of NBS 987 in each session are both reported in this study, see **Table 3**
248 **and 4**. An internal carbonate standard (N1, modern shell) was processed along with
249 sample leachates and its multi-run average is 0.70918 (2sd = 1.8×10^{-5} , n=10). A

250 procedural blank was included in each batch of samples, and Sr quantities (below 0.1
251 ng) were negligible compared to the analyte signal.

252 For C, O isotope analysis, powdered carbonate was analyzed at the Bloomsbury
253 Environmental Isotope Facility (BEIF) at University College London on a continuous-
254 flow (ThermoFisher Delta V) mass spectrometer linked to a Gas Bench II device.

255 External error (1σ) from standards (NBS19) was better than $\pm 0.04\text{‰}$ for $\delta^{13}\text{C}$ and \pm
256 0.05‰ for $\delta^{18}\text{O}$. All values are reported using the Vienna Pee Dee Belemnite notation
257 (VPDB) relative to NBS19 ($\delta^{13}\text{C}=1.95\text{‰}$, $\delta^{18}\text{O}=-2.2\text{‰}$).

258 **4. Results**

259 **4.1. Step leaching Sr isotopic and elemental variation**

260 $^{87}\text{Sr}/^{86}\text{Sr}$ and elemental (Mg/Ca, Mn/Sr, Sr/Ca, Rb/Sr, Ba/Ca, K/Ca, Al/Ca, Fe/Ca)
261 ratios, and cumulative % carbonate dissolution for all leaching steps for samples (J95,
262 G99, K46, G90, HXSZ4) and two rock standards (LS19, 88a) are shown in **Table 3**,
263 **Fig. 1-4.**

264 For all types of rocks, $^{87}\text{Sr}/^{86}\text{Sr}$ ratios in step 0 (1 M NH_4AC prewash) show very
265 high (or the highest) values. The pure limestone sample (LS19) exhibits lowest Sr
266 isotope ratios through the three middle leachates (S1-S3), corresponding to the middle
267 ~5%-70% carbonate dissolution, before rising in the final two leaching steps. The
268 lowest Sr isotope values in S1-S3 are associated with lower Mg/Ca, Mn/Sr, Rb/Sr,
269 K/Ca, Ba/Ca, Al/Ca, Fe/Ca ratios, and a higher Sr/Ca ratio than both the prewash and
270 the last two leachates. The middle three values of LS19 measured in this study
271 (0.70543 ± 0.00003) are consistent with what has been reported ($0.705439 \pm$
272 0.000003) by Zhou et al., (2020) within error.

273 Sequential dissolution of argillaceous and dolomitic limestone (SDL and HDL),
274 following the NH_4Ac prewash, results in a minimum $^{87}\text{Sr}/^{86}\text{Sr}$ value in S1 (c. 10% ~
275 30% carbonate dissolution), an increase in S2 and a dramatic increase in the last two
276 steps. The lowermost Sr isotope ratios of argillaceous and dolomitic samples range
277 from 0.70503 to 0.70533, similar to the reported seawater range during 1.60-1.55 Ga
278 (0.7046-0.7056; e.g., Ray et al., 2003; Kuznetsov et al., 2008; Bellefroid et al., 2018;
279 Tan et al., 2020). In general, Sr isotope ratios are seen to be higher when elemental
280 ratio indicators of alteration, such as Mg/Ca, Rb/Sr, Ba/Ca, and K/Ca, are higher.

281 From S1 onwards, Sr/Ca shows a gradually decreasing trend, while Mn/Sr shows an
282 increasing trend. Al/Ca and Fe/Ca ratios rise more clearly only after S6.

283 The $^{87}\text{Sr}/^{86}\text{Sr}$ values of the pure dolostone sample (88a) have two apparent dips at
284 S1-S2 and S7-S8, which correspond to 20% ~ 30% and 70% ~ 80% of carbonate
285 dissolution, respectively, with the lowest value found in S7-S8 (0.710043) (**Fig. 4A**).

286 Mg/Ca increases gradually from S0 to S9. Mn/Sr, Sr/Ca, Rb/Sr, Ba/Ca and K/Ca
287 ratios decrease after S0 and remain stable since S1, which are mirrored by Al/Ca,
288 Fe/Ca ratios.

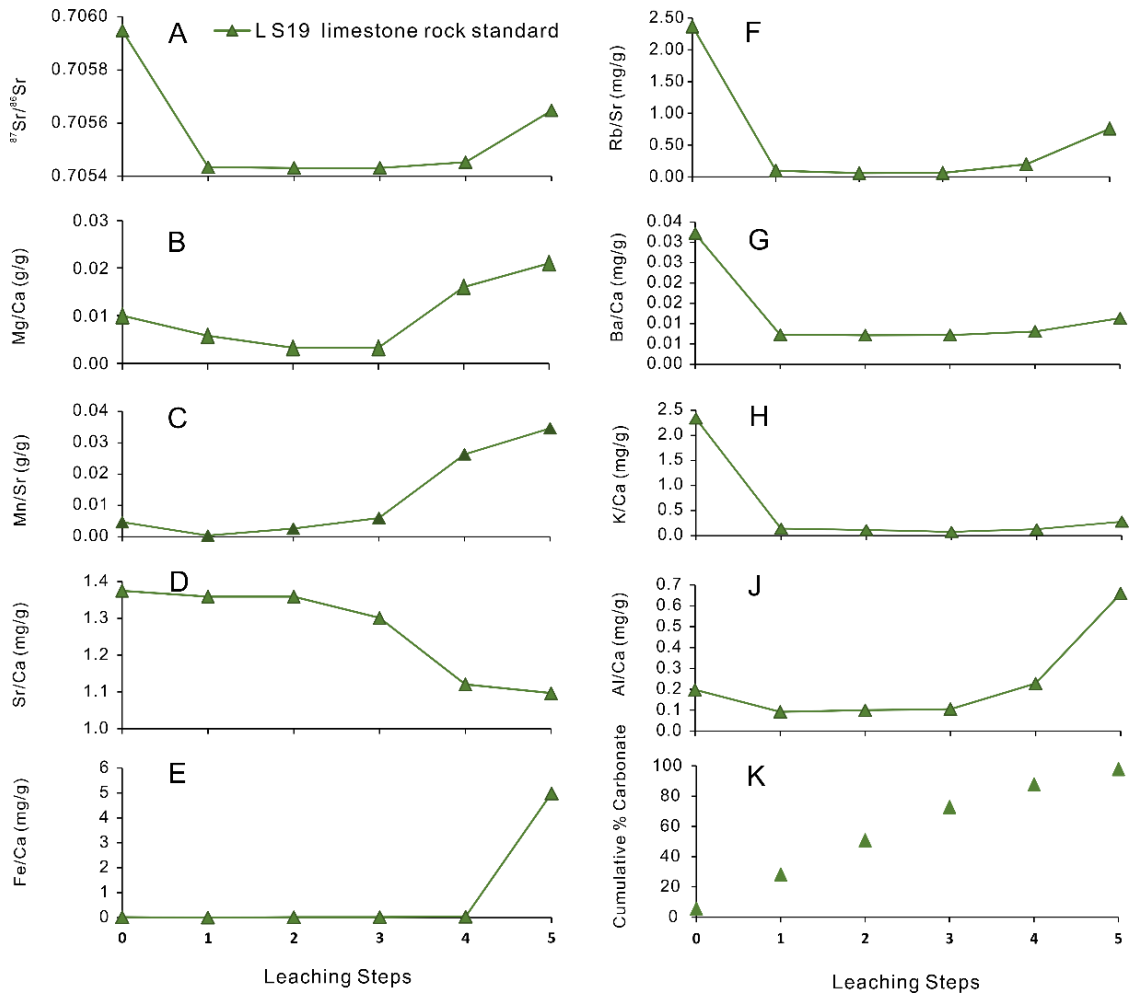


Fig. 1. Leaching pattern of pure limestones (LST) standard LS19

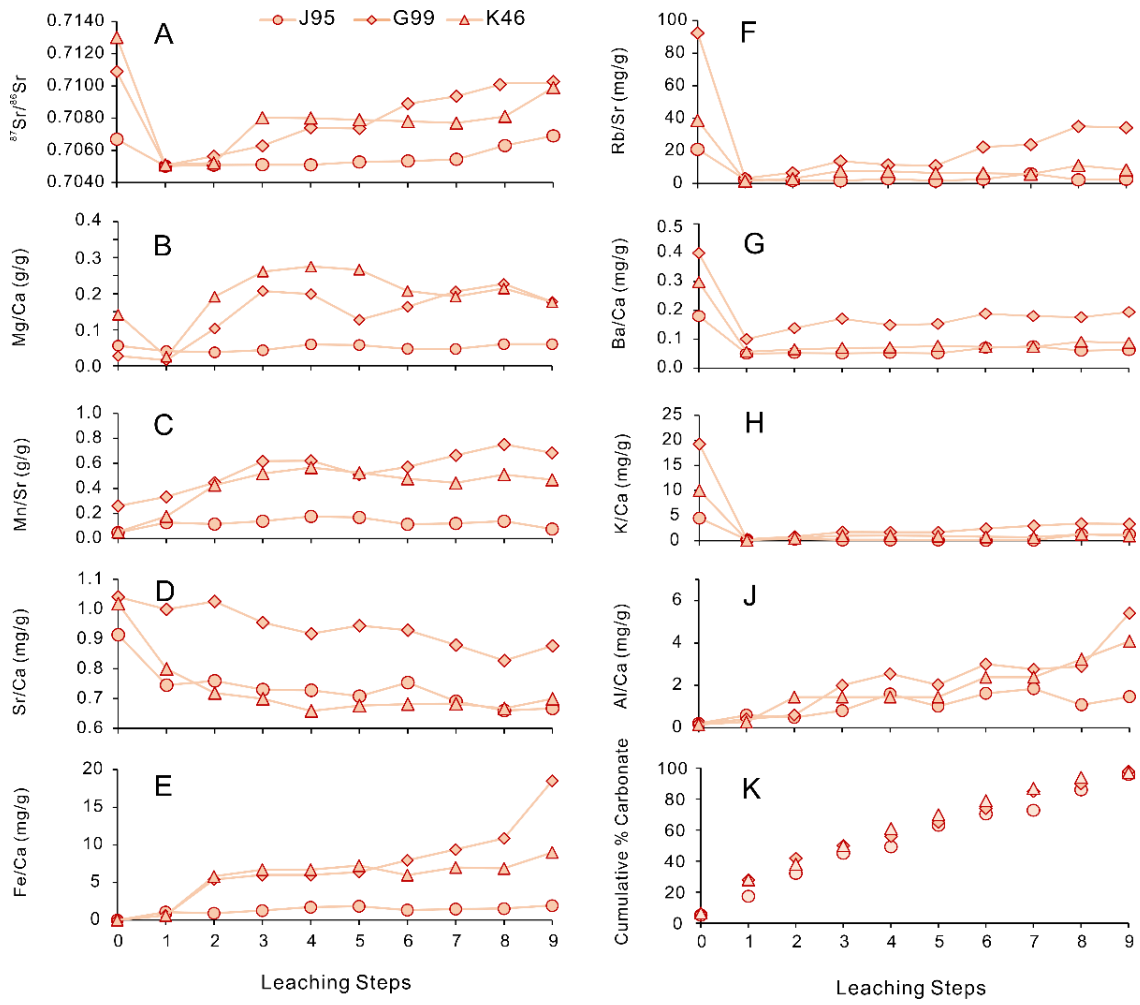


Fig. 2. Leaching pattern of argillaceous and slightly dolomitic limestones (SDL)

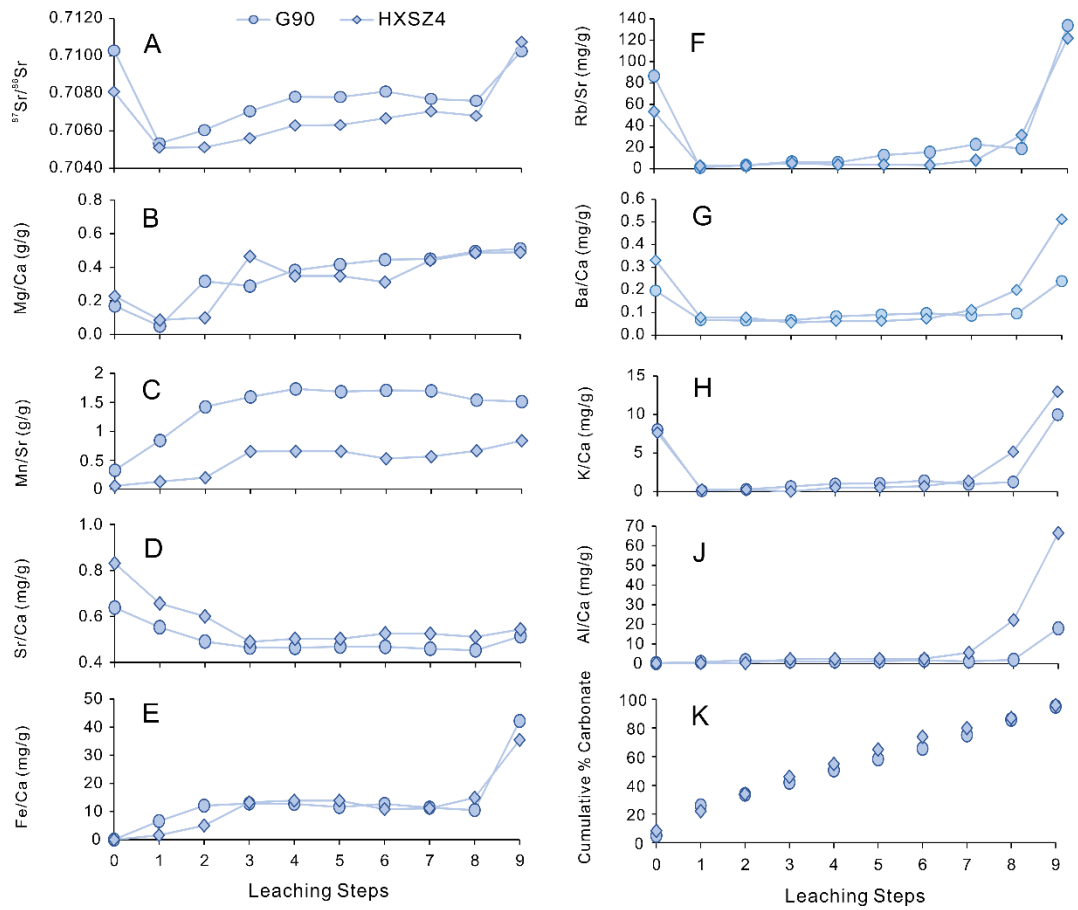


Fig. 3. Leaching pattern of argillaceous and highly dolomitic limestones (HDL).

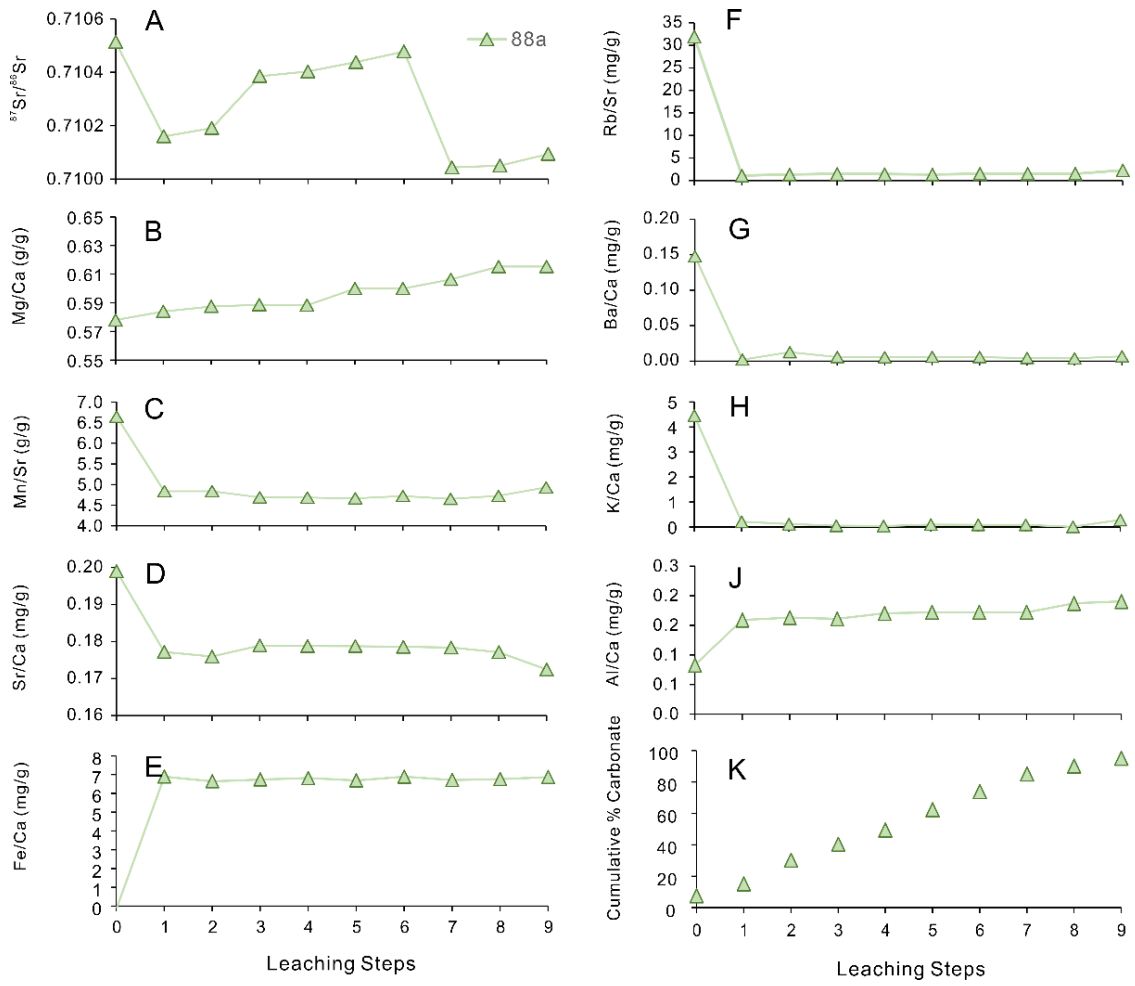


Fig. 4. Leaching pattern of pure dolostone rock standard 88a (DST).

Sample	Carbonate dissolved (cumulative)	$^{87}\text{Sr}/^{86}\text{Sr}$	2se	2sd	Sample	Carbonate dissolved (cumulative)	$^{87}\text{Sr}/^{86}\text{Sr}$	2se	2sd
LS19-0	5.64%	0.70595	2.54E-05	3.07E-05	G90-0	5.02%	0.71029	2.32E-05	3.03E-05
LS19-1	28.34%	0.70543	2.00E-05	3.07E-05	G90-1	25.93%	0.70533	2.18E-05	3.03E-05
LS19-2	50.84%	0.70543	2.08E-05	3.07E-05	G90-2	33.77%	0.70580	2.18E-05	3.03E-05
LS19-3	72.89%	0.70543	2.30E-05	3.07E-05	G90-3	41.96%	0.70704	1.95E-05	3.03E-05
LS19-4	87.93%	0.70545	2.20E-05	3.07E-05	G90-4	50.69%	0.70781	2.50E-05	3.03E-05
LS19-5	98.00%	0.70565	2.54E-05	3.07E-05	G90-5	58.38%	0.70780	2.46E-05	3.03E-05
J95-0	5.16%	0.70669	2.72E-05	3.07E-05	G90-6	65.64%	0.70810	1.92E-05	3.03E-05
J95-1	17.34%	0.70503	2.10E-05	3.07E-05	G90-7	75.14%	0.70770	2.32E-05	3.03E-05
J95-2	32.20%	0.70509	2.32E-05	3.07E-05	G90-8	86.00%	0.70760	1.84E-05	3.03E-05
J95-3	40.10%	0.70511	2.04E-05	3.07E-05	G90-9	95.00%	0.71025	2.38E-05	3.03E-05
J95-4	49.29%	0.70510	1.77E-05	3.07E-05	HXSZ4-0	8.35%	0.70808	2.38E-05	3.03E-05
J95-5	63.12%	0.70529	2.08E-05	3.07E-05	HXSZ4-1	22.00%	0.70520	2.56E-05	3.03E-05
J95-6	70.49%	0.70534	1.68E-05	3.07E-05	HXSZ4-2	34.00%	0.70522	2.40E-04	3.03E-05
J95-7	77.78%	0.70544	2.14E-05	3.07E-05	HXSZ4-3	46.00%	0.70561	2.00E-05	3.03E-05
J95-8	86.00%	0.70630	2.08E-05	3.07E-05	HXSZ4-4	55.00%	0.70629	2.06E-05	3.03E-05
J95-9	96.00%	0.70690	1.93E-05	3.07E-05	HXSZ4-5	65.00%	0.70631	1.80E-05	3.03E-05
G99-0	6.09%	0.71089	2.26E-05	3.07E-05	HXSZ4-6	74.00%	0.70667	1.90E-05	3.03E-05
G99-1	28.00%	0.70508	2.52E-05	3.07E-05	HXSZ4-7	80.00%	0.70704	1.82E-05	3.03E-05
G99-2	41.88%	0.70525	2.96E-05	3.07E-05	HXSZ4-8	87.00%	0.70680	2.50E-05	3.03E-05
G99-3	50.00%	0.70628	2.72E-05	3.07E-05	HXSZ4-9	96.00%	0.71075	2.82E-05	3.03E-05
G99-4	56.00%	0.70741	2.48E-05	3.07E-05	88-0	1.10%	0.71051	2.46E-05	3.03E-05
G99-5	65.00%	0.70737	2.04E-05	3.07E-05	88-1	13.87%	0.71016	1.38E-05	3.03E-05

G99-6	74.00%	0.70889	2.00E-05	3.07E-05	88-2	29.05%	0.71016	2.12E-05	3.03E-05
G99-7	85.00%	0.70936	2.18E-05	3.07E-05	88-3	39.64%	0.71039	2.56E-05	3.03E-05
G99-8	90.00%	0.71017	2.32E-05	3.07E-05	88-4	48.63%	0.71040	2.50E-05	3.03E-05
G99-9	98.00%	0.71017	2.90E-05	3.07E-05	88-5	61.29%	0.71044	2.56E-05	3.03E-05
K46-0	6.51%	0.71301	2.00E-05	3.07E-05	88-6	73.36%	0.71048	1.81E-05	3.03E-05
K46-1	28.00%	0.70507	2.96E-05	3.07E-05	88-7	83.97%	0.71004	2.38E-05	3.03E-05
K46-2	38.00%	0.70522	2.20E-05	3.07E-05	88-8	90.63%	0.71005	2.78E-05	3.03E-05
K46-3	50.00%	0.70803	2.36E-05	3.07E-05	88-9	93.81%	0.71009	2.30E-05	3.03E-05
K46-4	61.00%	0.70800	2.92E-05	3.07E-05					
K46-5	70.00%	0.70790	2.42E-05	3.07E-05					
K46-6	79.00%	0.70780	2.74E-05	3.07E-05					
K46-7	87.00%	0.70770	2.10E-05	3.07E-05					
K46-8	94.00%	0.70810	2.12E-05	3.07E-05					
K46-9	97.00%	0.70990	2.08E-05	3.07E-05					

Table 3. $^{87}\text{Sr}/^{86}\text{Sr}$ and cumulative carbonate dissolution in each step of each sample. The internal standard error (2se) for each sample and standard deviation (2sd) for repeat measurements of NBS 987 in each session are reported here. The lowest value (within 2sd) for each sample is highlighted by ***bold and italic***. See **Table S1 in Supplementary Materials** for major and trace element data.

290 4.2. Step leaching REY pattern

291 To help understand the leaching pattern of Sr isotopes for argillaceous and
292 dolomitic limestones, we also examined their step-leaching REY pattern (**Fig. 5,**
293 **Table S2 in Supplementary Materials**). Supernatants of ammonium acetate prewash
294 exhibit a non-seawater pattern, either being flat or displaying a positive Eu anomaly.
295 Ba/Sm ratios show a strong correlation with $\text{Eu}_{\text{sn}}/\text{Eu}^*_{\text{sn}}$ for all argillaceous and
296 dolomitic limestones, strongly implying that Eu anomalies in the S0 resulted from
297 BaO interference in the ICP-MS (Jarvis et al., 1989), while no such correlation was
298 observed for other leaching steps (**Fig. 6**). A seawater-like REY pattern occurs in S1
299 for almost all samples but tends to be flat in the subsequent leaching steps. The only
300 exception is G99, which shows a non-seawater pattern and a negative Eu anomaly
301 throughout all leaching steps. The Y/Ho ratios of the argillaceous and dolomitic
302 limestone in each leaching step are shown in **Fig. 7**. All samples display a Y/Ho
303 ratio >36 in S1, and then the ratio gradually decreases in subsequent steps.

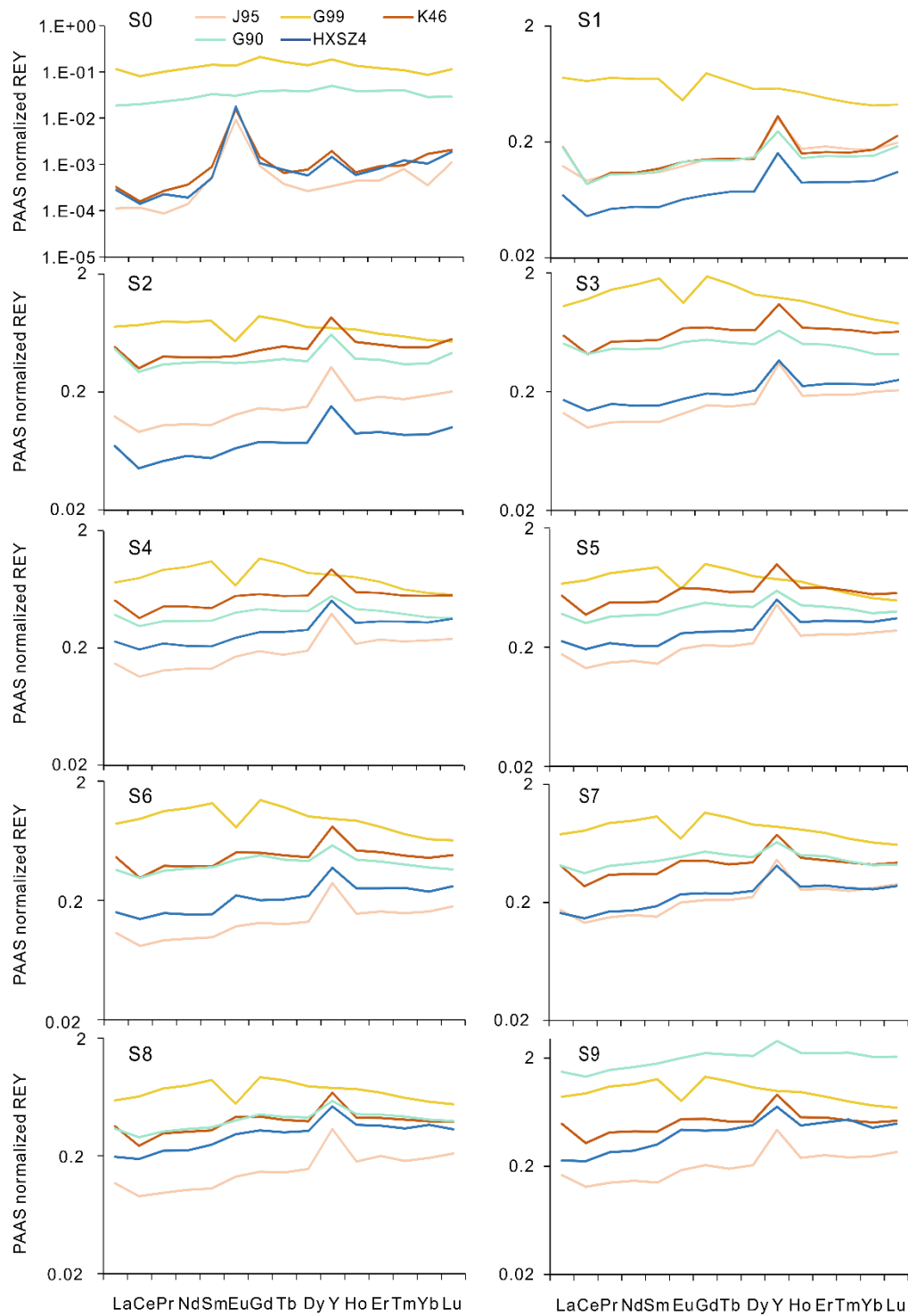


Fig. 5. Ten-step REY leaching pattern for argillaceous and dolomitic limestones. Each plot shows each step, and lines with different colours represent different samples. All plots are in log scale. Except for G99, all samples show the seawater pattern in S1 (some also in S2).

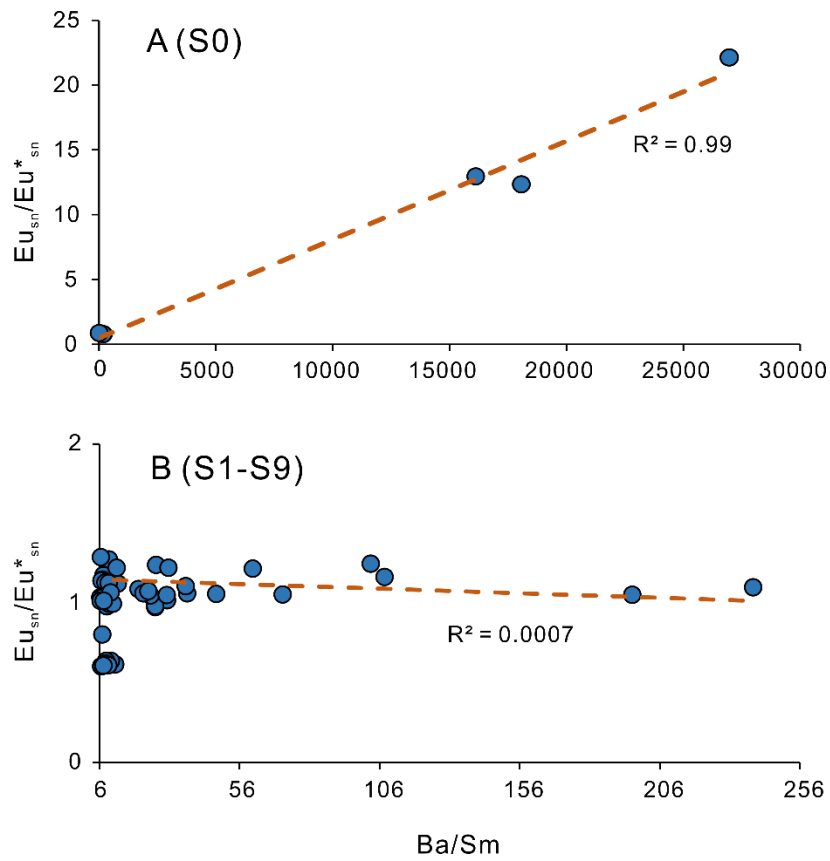


Fig. 6. Crossplots of Ba/Sm and Eu_{sn}/Eu_{sn}^* for 5 argillaceous and dolomitic limestones. A). Crossplot of Ba/Sm and Eu_{sn}/Eu_{sn}^* for S0 (NH₄Ac prewash) shows a strong correlation; B). Crossplot of Ba/Sm and Eu_{sn}/Eu_{sn}^* for S1-S9 shows no correlation.

$$Eu_{sn}/Eu_{sn}^* = 2 * [Eu]_{sn} / ([Sm]_{sn} + [Gd]_{sn}); \text{sn: shale normalized.}$$

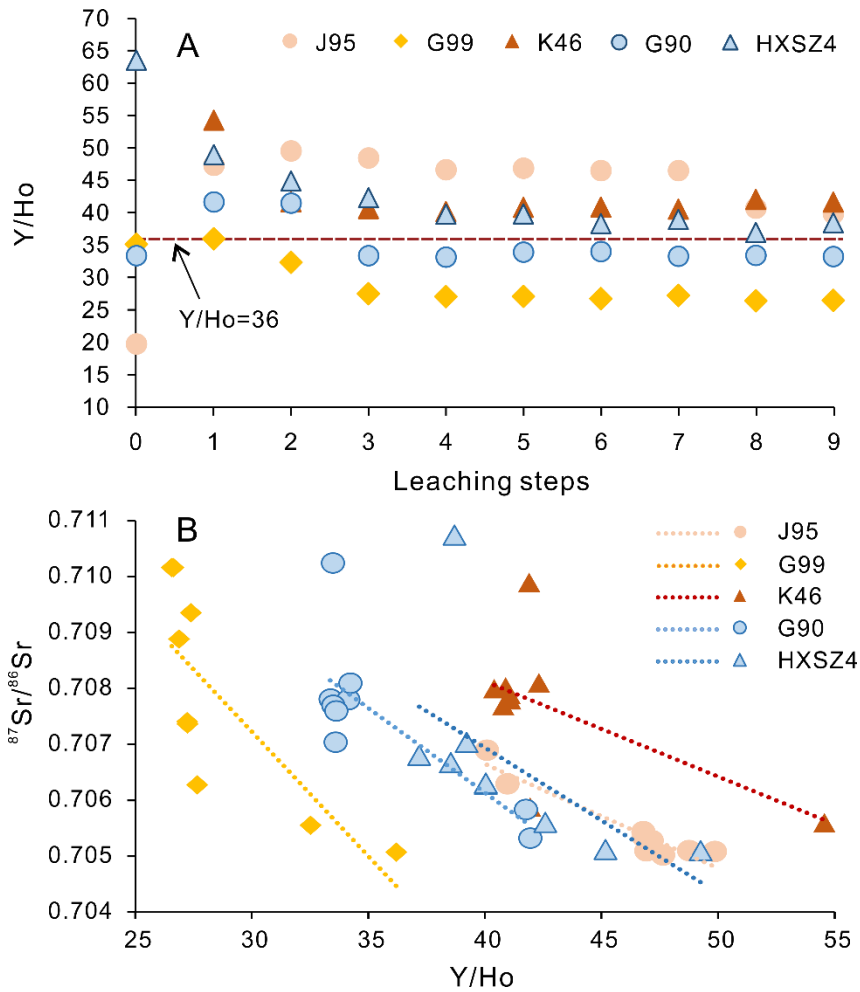


Fig.7. A). Y/Ho ratios in each leaching step of each sample. All samples in S1 show Y/Ho > 36 (seawater signal; less clay contamination). B). Cross-plot of Sr isotopes versus Y/Ho in each leaching step of each sample. A negative correlation was observed for each sample.

304 **4.3. Leaching methods' comparison results**

305 As mentioned before (section 3.1.2), 20 carbonate samples with various purity are
 306 selected to test the three different leaching methods: *Method 1* - target the first 10% ~
 307 30% after NH₄Ac prewash (this study); *Method 2* - preleach 30%, target the next 30%
 308 (Bailey et al., 2000; Li et al., 2011); *Method 3* - preleach 60%-70%, target the next
 309 ~20% (Liu et al., 2013; Li et al., 2020). Sr isotope results and bulk carbonate
 310 information for each sample are shown in **Table 4** and **Fig. 8**. For pure limestone

311 (HXS1), no significant differences are evident between the three different leaching
 312 cut-offs (i.e., the disparities are within measurement errors). For some very
 313 argillaceous samples (carbonate content $\leq \sim 50\%$) such as G94 and G97, applying
 314 higher leaching cut-offs (i.e., methods 2 and 3) would increase the Sr isotope ratios
 315 dramatically (up to 0.009 compared with targeting the first 10% ~ 30% after
 316 prewash). Relatively pure dolomitic limestones (% carbonate $> 80\%$ and $0.025 <$
 317 $Mg/Ca < 0.6$) also tend to reach the lowest values using method 1, the method this
 318 study recommends, although adjusting cut off points would not produce the more
 319 extreme differences seen in very argillaceous samples. When $Mg/Ca > 0.4$, the
 320 situation becomes quite complicated, i.e., the lowest value could be generated by any
 321 of the leaching methods, but no near-seawater values are observed.

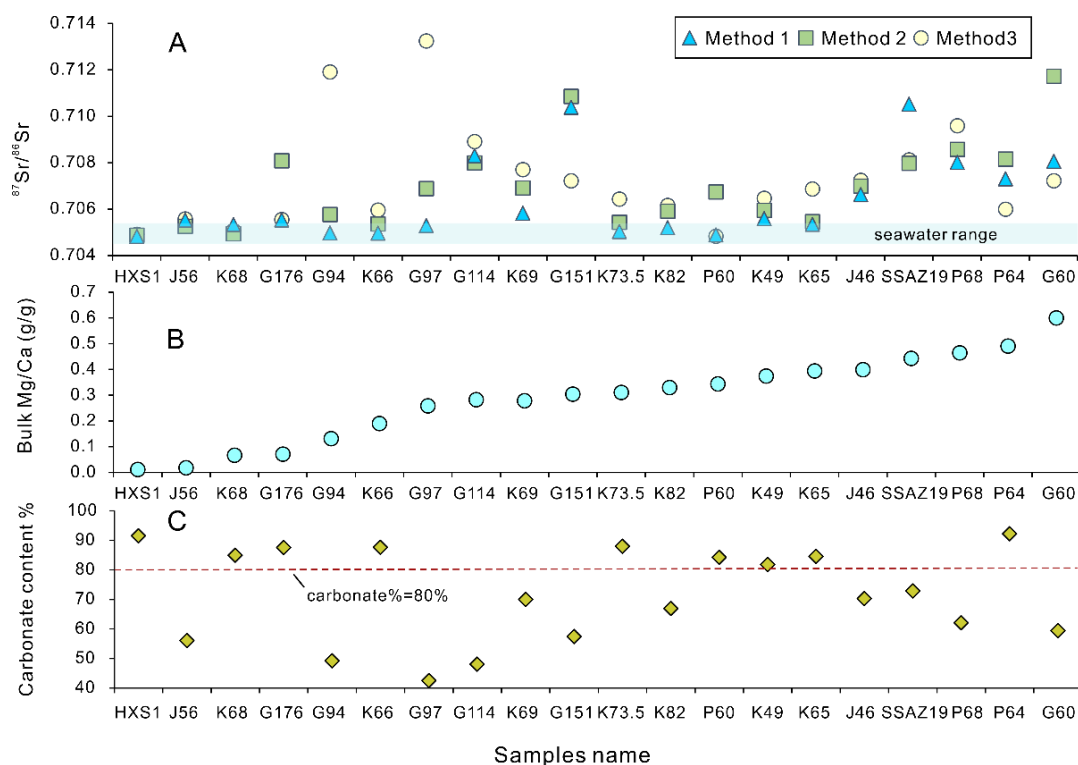


Fig. 8. A). Sr isotope results by applying different leaching Methods to each sample. Blue horizontal bar presents the possible seawater range from ~ 0.7046 to ~ 0.7056 of the Member III of Gaoyuzhuang Fm (see section 2.1 for details). **B).** Bulk Mg/Ca ratios of samples range

from 0.01 to 0.6. **C).** Carbonate content of each sample. Redline shows % carbonate = 80%, which divides samples into high purity (> 80%) and low purity (< 80%).

Samples	$^{87}\text{Sr}/^{86}\text{Sr}$			Bulk rock			
	<i>Method 1</i>	<i>Method 2</i>	<i>Method 3</i>	Carbonate content (%)	Mg/Ca (g/g)	Mn/Sr (g/g)	[Sr/(Ca+Mg)] (ppm)
HXS1	<i>0.70487 (2)</i>	<i>0.70488 (2)</i>	<i>0.70488 (2)</i>	91.49	0.01	0.00	8295.27
J56	<i>0.70523 (2)</i>	<i>0.70526 (3)</i>	0.70558 (2)	56.06	0.02	0.31	579.20
K68	<i>0.70493 (2)</i>	<i>0.70495 (1)</i>	0.70508 (2)	84.95	0.07	0.35	521.65
G176	<i>0.70653 (2)</i>	0.70809 (2)	<i>0.70655 (2)</i>	87.55	0.07	3.04	192.74
G94	<i>0.70498 (1)</i>	0.70577 (3)	0.71191 (2)	49.20	0.13	0.23	1106.69
K66	<i>0.70496 (2)</i>	0.70536 (2)	0.70596 (2)	87.62	0.19	0.30	662.06
G97	<i>0.70509 (2)</i>	0.70689 (2)	0.71325 (3)	49.52	0.26	0.48	662.05
G114	0.70829 (2)	<i>0.70800 (2)</i>	0.70891 (2)	48.06	0.28	2.22	404.09
K69	<i>0.70583 (3)</i>	0.70692 (2)	0.70771 (2)	70.00	0.28	0.40	779.79
G151	<i>0.71038 (3)</i>	0.71086 (3)	<i>0.70723 (2)</i>	57.45	0.30	3.82	233.93
K73.5	<i>0.70503 (2)</i>	<i>0.70505 (1)</i>	0.70643 (2)	88.00	0.31	0.44	842.47
K82	<i>0.70520 (2)</i>	0.70592 (2)	0.70616 (1)	66.94	0.33	0.56	442.54
P60	<i>0.70483 (2)</i>	0.70674 (1)	<i>0.70484 (2)</i>	84.20	0.34	1.69	218.06
K49	<i>0.70559 (2)</i>	0.70595 (2)	0.70647 (2)	81.80	0.37	0.84	389.22
K65	<i>0.70535 (1)</i>	0.70546 (2)	0.70687 (2)	84.59	0.39	0.67	499.80
J46	<i>0.70662 (2)</i>	0.70700 (2)	0.70724 (2)	70.28	0.40	4.43	261.99
SSAZ19	0.71053 (2)	<i>0.70798 (1)</i>	0.70812 (1)	72.86	0.44	2.00	301.35
P68	<i>0.70802 (2)</i>	0.70857 (2)	0.70959 (2)	62.13	0.46	3.34	178.26
P64	0.70731 (2)	0.70816 (1)	<i>0.70600 (3)</i>	92.21	0.49	2.89	145.95
G60	0.70806 (2)	0.71173 (2)	<i>0.70723 (1)</i>	59.46	0.60	4.29	124.37

Table 4. $^{87}\text{Sr}/^{86}\text{Sr}$ results of applying different cut-offs to samples with various bulk rock information. Note that the number in the bracket represents the 2se in the least digit. ***Bold and italic*** highlight the lowest value (within 2sd) among three different leaching methods (2sd = 3.11E-05).

322 **5. Discussion**

323 **5.1. Explanations of step-leaching Sr isotope and elemental variations**

324 The leaching step showing the lowest, and likely most pristine Sr isotope ratios
325 may correspond to the effective isolation of either the clay-free carbonate fraction
326 and/or the least altered carbonate phase in a given sample. Rb, K, and Al
327 concentrations are typical indicators of aluminosilicate Sr contamination (Banner et
328 al., 1988; McArthur, 1994; Montañez et al., 1996). Rb and K can both be used to track
329 clay surface-bound Sr released by ion exchange as well as detrital / authigenic clay
330 dissolution. By contrast, Al might not be a suitable proxy for Sr released from clay
331 surfaces due to its insoluble nature (Bellefroid et al., 2018), but it is a strong sign of
332 aluminosilicate dissolution (Wierzbowski et al., 2012). Mg/Ca is used to quantify the
333 relative contribution of calcite and dolomite during leaching steps and the degree of
334 dolomitization in a sample. Mn/Sr, Fe/Ca and Sr/Ca are often used as indices of
335 alteration, and Mn/Sr, Fe/Ca are generally expected to be higher, while Sr/Ca is
336 considered to be lower in diagenetically altered samples than in coeval seawater
337 (Banner and Hanson, 1990; Gorokhov et al., 1995; Kaufman and Knoll, 1995). This
338 general relationship is complicated by variable redox conditions, diagenetic fluids,
339 and mineralogy. For instance, compared with calcite, dolomite generally has a greater
340 preference for Fe and Mn (Mazzullo, 1992) and a lower preference for Sr
341 (Vahrenkamp and Swart, 1990). Apart from diagenetic phases, the stepwise leaching
342 patterns of Mn/Sr and Fe/Ca might also indicate the dissolution of non-carbonate
343 phases such as Fe-Mn oxides (e.g., Zhang et al., 2015)

344 5.1.1. Argillaceous and dolomitic limestones

345 5.1.1.1. Similarities among samples

346 All argillaceous and dolomitic limestones exhibit a similar Sr isotope leaching
347 pattern, i.e., reaching a nadir in S1, and then rising through subsequent steps. A
348 comparable pattern was previously reported by Bellefroid et al., (2018) on limestones
349 of the Dhaiqa and Tieling formations, where it was referred to as a "V"-shaped
350 pattern. The extremely radiogenic Sr and high Rb/Sr, K/Ca ratios of the first leaching
351 step (S0) by ammonium acetate are contributed to significantly by Sr in ion exchange
352 sites in clay minerals and trace metals adsorbed on mineral surfaces (Morton, 1985;
353 Gao, 1990; Bailey et al., 2000). The dramatic drop of Rb/Sr, K/Ca and $^{87}\text{Sr}/^{86}\text{Sr}$ in the
354 following step (S1, in some cases S2) indicates that pre-cleaning has effectively
355 removed this weakly surface-bound Sr. The increase in Rb/Sr, K/Ca, and Al/Ca ratios
356 and more radiogenic $^{87}\text{Sr}/^{86}\text{Sr}$ from S2, and especially after S6, most likely implies
357 partial dissolution of residual aluminosilicate, considering the samples' argillaceous
358 lithology. Intriguingly, we found that Ba/Ca follows a similar pattern and exhibits a
359 strong linear correlation with Rb/Sr ($R^2 > 0.95$; **Fig. 9**). Previous research found that
360 clay is one of the main Ba-carriers in marine sediments (Rutten and de Lange, 2002;
361 Gonneea and Paytan, 2006). Therefore, the strong correlation between Rb and Ba
362 might support the use of Ba/Ca ratios as indicators of clay contamination. Low Mg/Ca
363 ratios (all below 0.1) in S1 for all argillaceous and dolomitic limestones indicate that
364 the calcite proportion was leached out before dolomite as calcite reacts much faster
365 with acid than dolomite. Gradually increasing Mg/Ca, Mn/Sr and Fe/Ca and
366 decreasing Sr/Ca after S1 demonstrate that the calcite proportion in S1 is the closest to
367 primary carbonate phase, which is released before secondary calcite, dolomite and
368 non-carbonate minerals are dissolved in subsequent leaching steps.

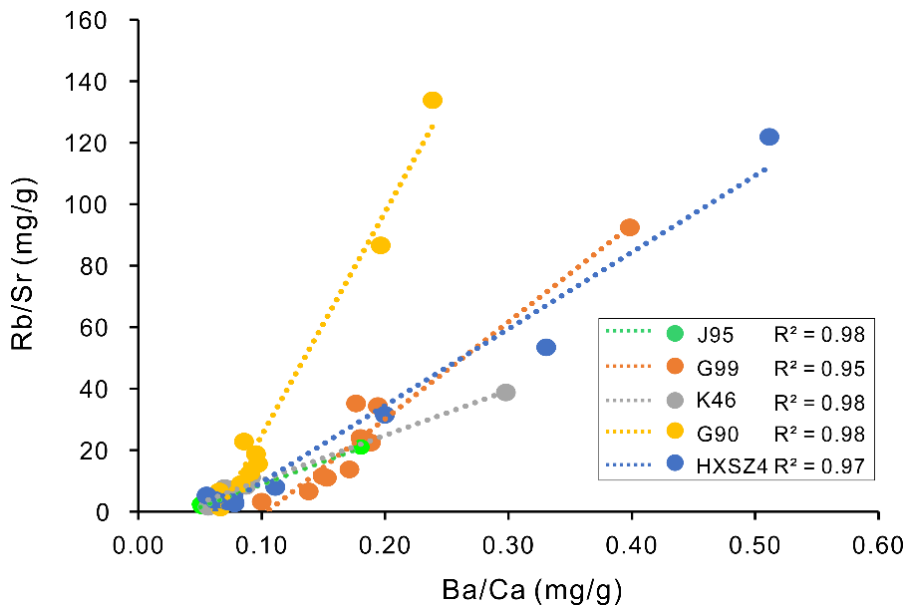


Fig. 9. Cross-plot of stepwise Rb/Sr versus Ba/Ca ratios for each argillaceous and dolomitic limestone. The correlation coefficient (R^2) of each sample is > 0.95 .

369 *5.1.1.2. Disparities among samples*

370 Slight differences still exist among samples, and more explanations could be
 371 investigated by cross plotting the stepwise elemental ratios (Rb/Sr, Mn/Sr and Mg/Ca)
 372 against Sr isotopes (**Fig. 10**). After reaching the minimal value in S1, J95, a slightly
 373 dolomitic limestone, shows a slower rebound to a higher value compared with other
 374 samples. The step leach Rb/Sr, Mn/Sr and Mg/Ca ratios of J95 show the weakest
 375 relationship with Sr isotopes (from S2 to S9) compared with other samples, which
 376 indicates that clay contamination and leaching of diagenetic phases did not influence
 377 the Sr isotope values immediately from S2 (**Fig. 10. A1-A3**). With a Mg/Ca ratio
 378 (0.06) close to limestone (< 0.025), and a carbonate content of $\sim 70\%$, J95 contains a
 379 relatively higher proportion of "clean and primary" calcite compared with the other
 380 four argillaceous and dolomitic limestones (G99, K46, G90, HXSZ4). In contrast, all
 381 samples except J95 show positive correlations between Rb/Sr and $^{87}\text{Sr}/^{86}\text{Sr}$ (**Fig. 10.**
 382 **B1-E1**), whereby the 'dirtiest' sample (G99) has the strongest correlation ($R^2=0.91$,
 383 **Fig. 10. B1**). This result demonstrates that for very argillaceous samples, the Sr

384 isotope leaching pattern is strongly and rapidly influenced by the dissolution of clay
385 minerals, immediately following the first leachate, even when using a weak acid.
386 Therefore, caution needs to be taken to avoid over-leaching when dealing with
387 argillaceous samples, while the first 10% ~ 30% after prewash would seem to
388 represent the cleanest portion. One possible factor that influences clay mineral
389 dissolution could be reaction time. The longer agitation in ultra-sonic bath and
390 reaction time since S3 (**Table 2**) could have contributed to the dissolution of more
391 clay minerals. This may indicate that when leaching dirty/muddy samples for Sr
392 isotopes analysis, shorter reaction time is preferable. Cross plots of stepwise Mg/Ca
393 and Mn/Sr versus Sr isotope ratios (**Fig. 10. A2-E2, A3-E3**) in most cases exhibit a
394 stronger covariation in highly dolomitic limestone (G90, HXSZ4) than for slightly
395 dolomitic limestones (J95, G99, K46), which possibly indicates that dissolution of the
396 dolomitized (likely more diagenetically altered) proportion is a more important
397 contributing factor that leads to increased $^{87}\text{Sr}/^{86}\text{Sr}$ ratios after S1 for samples with a
398 higher degree of dolomitization.

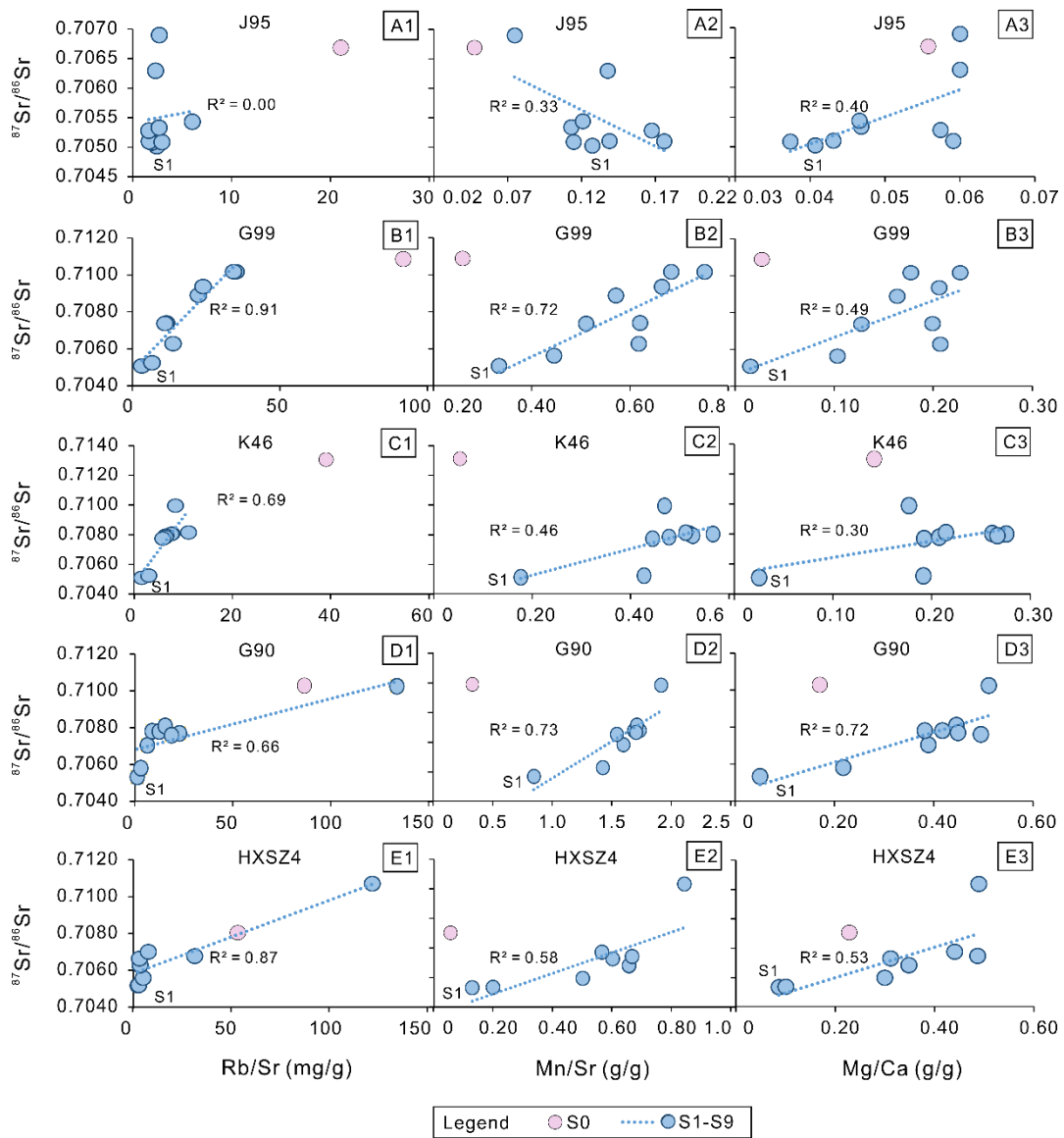


Fig. 10. Cross-plots of stepwise Rb/Sr, Mn/Sr and Mg/Ca ratios versus Sr isotopes for each argillaceous and dolomitic limestone. After S0 (prewash), correlations of Rb/Sr, Mn/Sr and Mg/Ca ratios with $^{87}\text{Sr}/^{86}\text{Sr}$ from S1 to S9 are shown in blue lines.

399

5.1.2. Two rock standards

400

Although a detailed discussion on SIS leaching methods for pure limestone and

401

dolostone samples is beyond the scope of this study, we wish to show how different

402

types of rocks behave by briefly demonstrating the leaching patterns of two rock

403

standards here. In pure limestone internal standard LS19, the “clean and primary”

404

proportion is much higher than in argillaceous and dolomitic limestones, as evidenced

405 by a consistent Sr isotope nadir alongside the lowest Mg/Ca and Mn/Sr ratios from S1
406 to S3, which corresponds to ~5% to 70% carbonate dissolution. This pattern is
407 consistent with previous studies on limestone samples (e.g., Bailey et al., 2000;
408 Bellefroid et al., 2018). Interestingly, the $^{87}\text{Sr}/^{86}\text{Sr}$ leaching pattern for CRM 88a
409 exhibits two low points in steps S1/S2, and S7/S8, respectively, although none of
410 these show seawater values as both sets of values are considerably higher than
411 contemporaneous seawater. Therefore, the leachates of CRM 88a might contain
412 calcite and dolomite formed at different stages of recrystallization. Nevertheless, the
413 lowest $^{87}\text{Sr}/^{86}\text{Sr}$ value of 88a from this study is significantly lower than reported by
414 Stammeier et al., (2020), in which the bulk sample was dissolved in 3 M HNO_3 .

415 **5.2. Comparison of $^{87}\text{Sr}/^{86}\text{Sr}$ with REY step-leaching pattern**

416 5.2.1. Clay contamination

417 The high sensitivity to clay contamination of both REY patterns and Sr isotopes
418 allows us to combine them to examine the validity of the leaching method for
419 argillaceous and dolomitic limestones. The step leaching REY patterns of all samples,
420 except for G99, show a seawater pattern in S1 (and some in S2), which is in line with
421 Sr isotope leaching patterns (lowest/seawater $^{87}\text{Sr}/^{86}\text{Sr}$ values in S1). This result is
422 also consistent with previous studies such as Tostevin et al., (2016) and Cao et al.,
423 (2020), which proposed that the early leaches contain more pristine seawater REY
424 signals for partially dolomitized and less pure limestones. The Y/Ho ratio is one of the
425 most effective approaches to recognizing terrigenous influences on seawater REY
426 distribution because Ho is scavenged two times faster than Y from the surface ocean
427 to the deep ocean (Nozaki et al., 1997). The Y/Ho ratio of seawater is consequently
428 almost twice that of the average upper continental crust (~26–28; Taylor and
429 McLennan, 1981; Kamber et al., 2005). $\text{Y}/\text{Ho} > 36$ is a commonly used threshold

430 value for seawater REY signals (e.g., Tostevin et al., 2016). The high Y/Ho ratios of
431 S1 (> 36, **Fig. 7A**), before gradually decreasing in subsequent steps, further confirms
432 our findings based on Sr isotopes, i.e. that step 1 leaches out the most primary portion
433 of the sample. The cross plot of stepwise $^{87}\text{Sr}/^{86}\text{Sr}$ with Y/Ho ratios of each sample
434 shows a negative covariation (either strong or weak, **Fig. 7B**), which is within
435 expectation as dissolution of clay minerals normally would increase $^{87}\text{Sr}/^{86}\text{Sr}$ values
436 while decreasing Y/Ho ratios. A conflicting story (i.e., a positive correlation between
437 $^{87}\text{Sr}/^{86}\text{Sr}$ and Y/Ho) was reported by (Verdel et al., 2018), in which the authors
438 attribute the disparity to the progressive dissolution of different combinations of
439 sources. Nevertheless, the high consistency between REY compositions and Sr
440 isotope leaching pattern in this study further confirmed a similar sensitivity of both
441 systems to clay contamination.

442 5.2.2. Organic matter activity and dolomitization

443 Even though the REY pattern is consistent with the Sr isotope leaching pattern in
444 most samples, an exception still exists in G99, the sample with a seawater like Sr
445 isotope value but without a seawater REY pattern. One difference between G99 and
446 other samples is that G99 contains high levels of organic compounds (total TOC of
447 1.3 wt %). It seems probable to us that during early diagenesis, degradation and
448 remineralization of organic matter released adsorbed REY into porewaters so it could
449 be incorporated into carbonate rocks, altering the original seawater REY pattern. The
450 potential for substantial, indirect influence from organic degradation on the original
451 carbonate REY pattern was also proposed in a recent study by Zhang and Shields,
452 (2022). Some research shows that organic matter preferentially absorbs LREE and
453 then releases it at depth during remineralization (Chen et al., 2015; Meyer et al.,
454 2021), but the understanding of REY in the biological system is still at an early stage;

455 thus, a range of REY patterns in organic matter might be expected (Zhang and
456 Shields, 2022). In contrast to REY patterns, the low Sr content of organic matter
457 means that it will have little influence on pore fluid Sr isotope composition.

458 In addition, the highly dolomitic limestones (G90, HXSZ4) also show marine-like
459 REY patterns in S1. This finding is consistent with the previously proposed argument
460 that dolomitization may not significantly alter REY patterns of carbonate rocks
461 (Banner et al., 1988; Zhang et al., 2015), although it might change Sr isotope
462 characteristics. Therefore, while REY and Sr isotopes in carbonates have similarities
463 (e.g., both are vulnerable to clay contamination), other factors (e.g., organic matter,
464 dolomitization) will have different impacts on these two systems.

465 5.2.3. Effectiveness of ammonium acetate prewash

466 Ammonium acetate prewash has been widely used for leaching protocols of
467 carbonate rocks for different proxies such as REY, Sr isotopes or Li isotopes to
468 remove the ion-exchangeable phase (Tessier et al., 1979; Bailey et al., 2000;
469 Kuznetsov et al., 2010; Liu et al., 2013; Pogge Von Strandmann et al., 2013; Cui et
470 al., 2015; Bellefroid et al., 2018; Cao et al., 2020). It was suggested that using dilute
471 acetic acid may remove Sr contamination more effectively (Bailey et al., 2000), but
472 for the argillaceous and dolomitic limestones, it might result in over-leach as only the
473 first 10%-30% should be extracted based on our study. In this case, using ammonium
474 acetate instead of acetic acid for pre-cleaning to remove adsorbed Sr and Rb would be
475 advisable as the *pH* neutral ammonium acetate would not attack as much carbonate
476 (less than 5%).

477 We agree that ammonium acetate might not remove all clay surface-bound
478 contamination (e.g., Bailey et al., 2000), but based on major and trace element, REY
479 and Sr isotope data (as discussed in previous sections), using an ammonium acetate

480 prewash is still an effective option. It is also worth noting that the reaction time may
481 play a significant role in the effectiveness of using ammonium acetate. It was
482 suggested that a 30-minute leaching time is sufficient to achieve maximum extraction
483 of adsorbed REE (Moldoveanu and Papangelakis, 2013; Cao et al., 2020), and this
484 reaction time was also applied in this study.

485 **5.3. Suitability of different leaching cut-offs for different types of samples**

486 The pure limestone (HXS1) shows no significant difference between the three
487 different leaching cut-offs (**Fig. 8 and Table 4**), which is consistent with the leaching
488 pattern of pure limestone LS19 (**Fig. 1A**). However, for very argillaceous samples (%
489 carbonate \leq ~50%) with Mg/Ca < 0.4, such as G94, G97, applying any higher pre-
490 leach cut-offs would produce a sizeable error compared with using the first 10%-30%
491 after prewash, similar to what we show for the leaching pattern of G99 (**Fig. 2A**). This
492 is because to extract the primary signal from carbonate rocks, two requirements must
493 be met simultaneously: "relatively clay-free" and "least altered", and the only possible
494 proportion for argillaceous and dolomitic limestones is the first 10%-30%, which
495 would be readily missed if samples are over-leached during pre-leach. By contrast, the
496 different leaching cut-offs for pure samples (carbonate content > 80%) with Mg/Ca <
497 0.4 (e.g., K66, K73.5, **Fig. 8**) do not produce as large a difference as the more
498 argillaceous samples. In general, most samples with Mg/Ca < 0.4 yield the
499 lowest/seawater Sr isotopic values with the first ~30% dissolution after prewash (**Fig.**
500 **8, Table 4**), which implies that for most of the limestones and slightly dolomitic
501 limestone samples of GYZ formation, the calcite proportion dissolved in the early
502 stage contains the primary marine signal. However, when Mg/Ca > 0.4, it is
503 unpredictable which method will yield the lowest $^{87}\text{Sr}/^{86}\text{Sr}$ value, and all lowest
504 values are higher than the proposed seawater value (**Fig. 8**). One possible contributing

505 factor is leaching out other calcite components, in the form of dedolomitization or
506 secondary veins and cements, especially in highly dolomitic limestones and
507 dolostones (e.g., Tostevin et al., 2016).

508 By comparison, targeting the first ~10%-30% carbonate after ammonium acetate
509 prewash appears to be the most appropriate method for SIS using a wide range of
510 carbonate, especially argillaceous and dolomitic limestones with detailed thresholds
511 described in session 5.4. The widely used cut-off for bulk carbonate (with 30%
512 preleach) is more suitable for limestones or pure dolomitic limestones than for other
513 rock types. Although our study and Liu et al., (2013, 2014) show pre-leaching of
514 60%-70% can obtain the lowest $^{87}\text{Sr}/^{86}\text{Sr}$ value for highly dolomitic limestones or
515 dolostones, our data present that the lowest Sr isotopic value of CRM 88a
516 ($\text{Mg}/\text{Ca}=0.6$) and other samples with $\text{Mg}/\text{Ca} > 0.4$ are higher than contemporaneous
517 seawater, therefore, without further tests, no recommendations can be made for these
518 types of samples.

519 **5.4. Recommended cut-offs for sample screening in SIS studies**

520 Based on our leaching tests and the application of three different methods to
521 twenty samples with different sample purity and dolomitization, we noticed that
522 samples with $\text{Mg}/\text{Ca} > 0.4$, $\text{Mn}/\text{Sr} > 2$, $[\text{Sr}] < 200$ ppm would be less likely to retain
523 the original seawater signal (i.e., all the lowest $^{87}\text{Sr}/^{86}\text{Sr}$ ratios from these types of
524 samples yielded from three leaching methods are higher than contemporaneous
525 seawater values). Cross-plots of Sr isotopes (lowest values among three methods)
526 versus bulk Mg/Ca , Mn/Sr , % carbonate, and $\text{Sr}/(\text{Ca}+\text{Mg})$ (**Fig. 11**) illustrate that
527 when $\text{Mg}/\text{Ca} < 0.25$, $[\text{Sr}] > 400$ ppm, $\text{Mn}/\text{Sr} < 2$, the success rate (the likelihood to
528 obtain seawater value) will be high. A previous study by Li et al., (2020) suggested
529 that samples with high purities ($> 75\%$ for limestones, $> 90\%$ for dolostones) are

530 more suitable for SIS. Even though sample purity influences the likelihood of
531 obtaining seawater values if the proposed seawater Sr isotopic ratio range is valid, our
532 data (**Fig. 8A and Fig. 11D**) show that our leaching method increases that likelihood
533 significantly, in 4 out of 6 cases with carbonate content < 70% when other thresholds
534 are met.

535 Our suggested thresholds here are based on the lowermost value among three
536 leaching methods for the 20 selected samples from the Gaoyuzhuang Formation. The
537 thresholds proposed from this study are in agreement broadly with previously
538 proposed thresholds by different studies (e.g., Bartley et al., 2001; Halverson et al.,
539 2007; Bold et al., 2016; Cox et al., 2016; Gibson et al., 2019; Zhou et al., 2020). We
540 agree that it is unlikely to have any single criterion for the robust screening of altered
541 samples because the post-depositional history varies from basin to basin (Bartley et
542 al., 2001; Melezhik et al., 2001; Halverson et al., 2007), but the consistency between
543 different research might provide a valuable reference for future Precambrian SIS
544 studies.

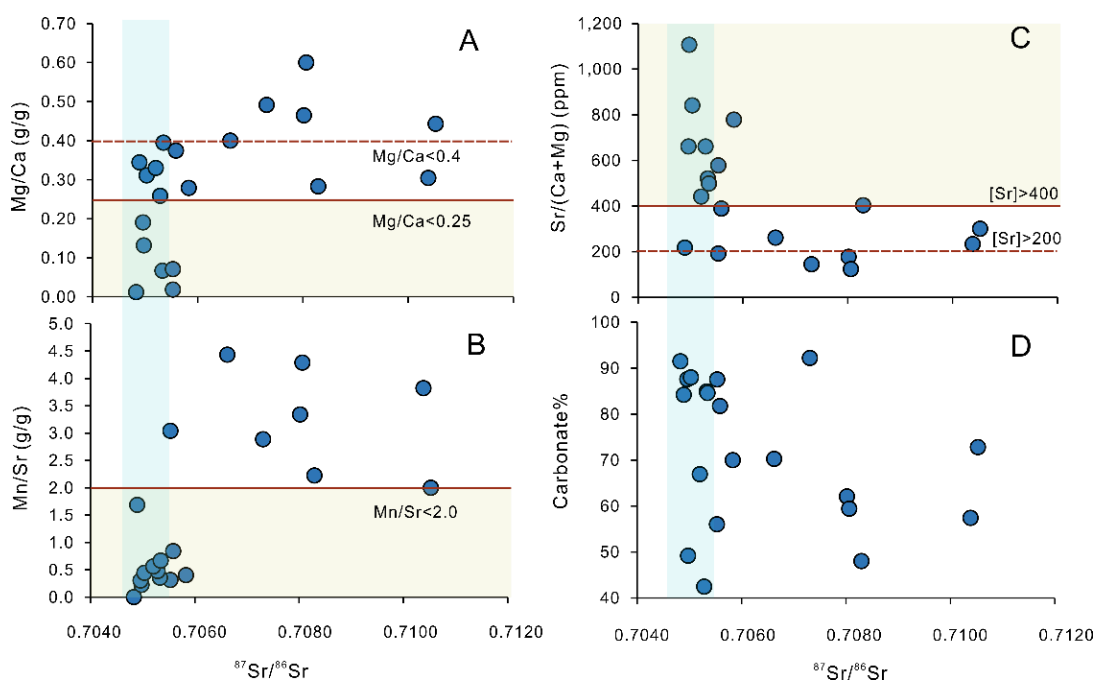


Fig. 11. Cross-plots bulk rock parameters of samples versus their lowermost Sr isotopes among three leaching cut-offs (see Table 4 for data). The blue shades show a seawater $^{87}\text{Sr}/^{86}\text{Sr}$ range (0.7046 ~ 0.7056) during this period. The yellow shades and red solid lines represent the thresholds highly probable for samples to yield seawater values. The red dash line shows recommended thresholds.

545 **6. Conclusions**

546 The major conclusions of this study are summarized below:

- 547 1) A Sr isotope leaching method for argillaceous and dolomitic limestones has
548 been developed, whereby the most effective approach involves extracting the
549 first 10% ~ 30% carbonate using weak acetic acid after ammonium acetate
550 prewash.
- 551 2) REY patterns of carbonate rocks, in agreement with Sr isotopes, exhibit the
552 most seawater-like patterns in the first leach after NH_4Ac prewash.
- 553 3) Organic matter remineralization during early diagenesis might influence the
554 REY patterns of carbonate rocks but will not have much influence on Sr
555 isotopes, while Sr isotopes are more vulnerable to dolomitization compared
556 with REY. Both $^{87}\text{Sr}/^{86}\text{Sr}$ and REY in carbonates are sensitive to clay
557 contamination.
- 558 4) Applying previously proposed leaching thresholds (e.g., preleach 30%~ 40%,
559 60%~70%) to the same argillaceous, dolomitic carbonate rocks leads to higher
560 $^{87}\text{Sr}/^{86}\text{Sr}$ values compared with targeting the first 10% ~ 30% directly after
561 NH_4Ac prewash. However, no significant differences were evident for high
562 purity, and low Mg/Ca limestones, which underlines the importance of
563 matching different sample types to the most appropriate dissolution method.

564 5) Thresholds for using Mg/Ca, [Sr] and Mn/Sr as screening tools for SIS study
565 are recommended: Mg/Ca < 0.4 (preferably < 0.25) (g/g); [Sr] > 200
566 (preferably > 400) ppm; Mn/Sr < 2. Our leaching method increases the
567 likelihood significantly of obtaining close to seawater Sr isotopic value for
568 samples with carbonate content < 70% when other thresholds are met.

569 **Acknowledgement**

570 The authors gratefully acknowledge funding support from NERC [grant numbers
571 NE/P013643/1, NE/R010129/1]; and Dean's Prize of the Faculty of Mathematical and
572 Physical Sciences, UCL. We would like to thank Graham A. Shields for helpful
573 discussion and suggestions on the manuscript and thank Fred T. Bowyer and Colin
574 Mettam for sample collections in the field.

575 **Appendix A. Supplementary material**

576 **References**

- 577 Bailey T. R., McArthur J. M., Prince H. and Thirlwall M. F. (2000) Dissolution
578 methods for strontium isotope stratigraphy: Whole rock analysis. *Chemical*
579 *Geology* **167**, 313–319.
- 580 Banner J. L. and Hanson G. N. (1990) Calculation of simultaneous isotopic and trace
581 element variations during water-rock interaction with applications to carbonate
582 diagenesis. *Geochimica et Cosmochimica Acta* **54**, 3123-3137.
- 583 Banner J. L., Hanson G. N. and Meyers W. J. (1988) Rare earth element and Nd
584 isotopic variations in regionally extensive dolomites from the Burlington-
585 Keokuk Formation (Mississippian): implications for REE mobility during
586 carbonate diagenesis. *Journal of Sedimentary Petrology* **58**.

587 Bartley J. K., Semikhatov M. A., Kaufman A. J., Knoll A. H., Pope M. C. and
588 Jacobsen S. B. (2001) Global events across the Mesoproterozoic-Neoproterozoic
589 boundary: C and Sr isotopic evidence from Siberia. *Precambrian Research* **111**,
590 165–202.

591 Bellefroid E. J., Planavsky N. J., Miller N. R., Brand U. and Wang C. (2018) Case
592 studies on the utility of sequential carbonate leaching for radiogenic strontium
593 isotope analysis. *Chemical Geology* **497**, 88–99.

594 Bold U., Smith E. F., Rooney A. D., Bowring S. A., Buchwaldt R., Dudás F. O.,
595 Ramezani J., Crowley J. L., Schrag D. P. and Macdonald F. A. (2016)
596 Neoproterozoic stratigraphy of the zavkhan terrane of Mongolia: The backbone
597 for cryogenian and early ediacaran chemostratigraphic records. *American*
598 *Journal of Science* **315**, 1–63.

599 Brand U., Azmy K., Tazawa J. I., Sano H. and Buhl D. (2010) Hydrothermal
600 diagenesis of Paleozoic seamount carbonate components. *Chemical Geology*
601 **278**, 173-185.

602 Broecker W. S. and Peng T. H. (1983) Tracers in the Sea. Eldigio Press, New York.

603 Burke W. H., Denison R. E., Hetherington E. A., Koepnick R. B., Nelson H. F. and
604 Otto J. B. (1982) Variation of seawater $^{87}\text{Sr}/^{86}\text{Sr}$ throughout Phanerozoic
605 time. *Geology* **10**, 516-519.

606 Cao C., Liu X. M., Bataille C. P. and Liu C. (2020) What do Ce anomalies in marine
607 carbonates really mean? A perspective from leaching experiments. *Chemical*
608 *Geology* **532**, 119413.

609 Banner J. L., Hanson G. N. and Meyers W. J. (1988) Rare earth element and Nd
610 isotopic variations in regionally extensive dolomites from the Burlington-

611 Keokuk Formation (Mississippian): implications for REE mobility during
612 carbonate diagenesis. *Journal of Sedimentary Petrology* **58**.

613 Chen J., Algeo T. J., Zhao L., Chen Z. Q., Cao L., Zhang L. and Li Y. (2015)
614 Diagenetic uptake of rare earth elements by bioapatite, with an example from
615 Lower Triassic conodonts of South China. *Earth-Science Reviews* **149**, 181-202.

616 Chen X., Zhou Y. and Shields G. A. (2022) Progress towards an improved
617 Precambrian seawater $87\text{Sr}/86\text{Sr}$ curve. *Earth-Science Reviews* **224**, 103869.

618 Cox G. M., Halverson G. P., Stevenson R. K., Vokaty M., Poirier A., Kunzmann M.,
619 Li Z. X., Denyszyn S. W., Strauss J. v. and Macdonald F. A. (2016) Continental
620 flood basalt weathering as a trigger for Neoproterozoic Snowball Earth. *Earth
621 and Planetary Science Letters* **446**, 89–99.

622 Cui H., Kaufman A. J., Xiao S., Zhu M., Zhou C. and Liu X. M. (2015) Redox
623 architecture of an Ediacaran ocean margin: Integrated chemostratigraphic ($\delta^{13}\text{C}$ -
624 $\delta^{34}\text{S}$ - $87\text{Sr}/86\text{Sr}$ - Ce/Ce^*) correlation of the Doushantuo Formation, South China.
625 *Chemical Geology* **405**, 48–62.

626 Cui H., Kaufman A. J., Zou H., Kattan F. H., Trusler P., Smith J., Yu. Ivantsov A.,
627 Rich T. H., al Qubsani A., Yazed A., Liu X. M., Johnson P., Goderis S., Claeys
628 P. and Vickers-Rich P. (2020) Primary or secondary? A dichotomy of the
629 strontium isotope anomalies in the Ediacaran carbonates of Saudi Arabia.
630 *Precambrian Research* **343**, 105720.

631 Elderfield H. (1986) Strontium isotope stratigraphy. *Palaeogeography,
632 Palaeoclimatology, Palaeoecology* **57**, 71-90.

633 Fairchild I. J., Spencer A. M., Ali D. O., Anderson R. P., Anderton R., Boomer I.,
634 Dove D., Evans J. D., Hambrey M. J., Howe J., Sawaki Y., Shields G. A.,

635 Skelton A., Tucker M. E., Wang Z. and Zhou Y. (2018) Tonian-Cryogenian
636 boundary sections of Argyll, Scotland. *Precambrian Research* **319**, 37–64.

637 Gao G. (1990) Geochemical and isotopic constraints on the diagenetic history of a
638 massive stratal, late Cambrian (Royer) dolomite, Lower Arbuckle Group, Slick
639 Hills, SW Oklahoma, USA. *Geochimica et Cosmochimica Acta* **54**, 1979-1989.

640 George V. Chilingar (1957) Classification of Limestones and Dolomites on Basis of
641 Ca/Mg Ratio. *SEPM Journal of Sedimentary Research* **27**, 187-189.

642 Gibson T. M., Wörndle S., Crockford P. W., Bui T. H., Creaser R. A. and Halverson
643 G. P. (2019) Radiogenic isotope chemostratigraphy reveals marine and
644 nonmarine depositional environments in the late Mesoproterozoic Borden Basin,
645 Arctic Canada. *GSA Bulletin* **131**, 1965–1978.

646 Gonnee M. E. and Paytan A. (2006) Phase associations of barium in marine
647 sediments. *Marine Chemistry* **100**, 124-135.

648 Gorokhov I., Semikhatov M., Baskakov A., Kutuyavin E., Mel’Nikov N., Sochava A.
649 and Turchenko T. (1995) Sr isotopic composition in Riphean, Vendian, and
650 Lower Cambrian carbonates from Siberia. *Stratigraphy and Geological*
651 *Correlation* **3**, 1–28.

652 Guo H., Du Y., Kah L. C., Huang J., Hu C., Huang H. and Yu W. (2013) Isotopic
653 composition of organic and inorganic carbon from the Mesoproterozoic Jixian
654 Group, North China: Implications for biological and oceanic evolution.
655 *Precambrian Research* **224**, 169-183.

656 Halverson G. P. (2007) A Neoproterozoic Chronology. *Neoproterozoic Geobiology*
657 *and Paleobiology* **27**, 231–271.

658 Halverson G. P., Dudás F. Ö., Maloof A. C. and Bowring S. A. (2007) Evolution of
659 the $87\text{Sr}/86\text{Sr}$ composition of Neoproterozoic seawater. *Palaeogeography,*
660 *Palaeoclimatology, Palaeoecology* **256**, 103–129.

661 Hawkesworth C. J., Cawood P. A. and Dhuime B. (2016) Tectonics and crustal
662 evolution. *GSA Today* **26**, 4–11.

663 Hodell D. A., Mead G. A. and Mueller P. A. (1990) Variation in the strontium
664 isotopic composition of seawater (8 Ma to present) : Implications for chemical
665 weathering rates and dissolved fluxes to the oceans. *Chemical Geology: Isotope*
666 *Geoscience Section* **80**, 291-307.

667 James R. H., Elderfield H. and Palmer M. R. (1995) The chemistry of hydrothermal
668 fluids from the Broken Spur site, 29°N Mid-Atlantic ridge. *Geochimica et*
669 *Cosmochimica Acta* **59**, 651-659.

670 Jarvis K. E., Gray A. L. and McCurdy E. (1989) Avoidance of spectral interference on
671 europium in inductively coupled plasma mass spectrometry by sensitive
672 measurement of the doubly charged ion. *Journal of Analytical Atomic*
673 *Spectrometry* **4**, 743-747.

674 Kah L. C., Lyons T. W. and Chesley J. T. (2001) Geochemistry of a 1.2 Ga carbonate-
675 evaporite succession, northern Baffin and Bylot Islands: Implications for
676 Mesoproterozoic marine evolution. *Precambrian Research* **111**, 203–234.

677 Kamber B. S., Greig A. and Collerson K. D. (2005) A new estimate for the
678 composition of weathered young upper continental crust from alluvial sediments,
679 Queensland, Australia. *Geochimica et Cosmochimica Acta* **69**, 1041-1058.

680 Kaufman A. J. and Knoll A. H. (1995) Neoproterozoic variations in the C-isotopic
681 composition of seawater: stratigraphic and biogeochemical implications.
682 *Precambrian Research* **73**, 27-49.

683 Kuznetsov A. B., Melezhik V. A., Gorokhov I. M., Melnikov N. N., Konstantinova G.
684 v., Kutyavin E. P. and Turchenko T. L. (2010) Sr isotopic composition of
685 Paleoproterozoic ¹³C-rich carbonate rocks: The Tulomozero Formation, SE
686 Fennoscandian Shield. *Precambrian Research* **182**, 300–312.

687 Kuznetsov A. B., Ovchinnikova G. v., Semikhatov M. A., Gorokhov I. M., Kaurova
688 O. K., Krupenin M. T., Vasil'eva I. M., Gorokhovskii B. M. and Maslov A. v.
689 (2008) The Sr isotopic characterization and Pb-Pb age of carbonate rocks from
690 the Satka formation, the Lower Riphean Burzyan Group of the southern Urals.
691 *Stratigraphy and Geological Correlation* **16**, 120–137.

692 Li D., Shields-Zhou G. A., Ling H. F. and Thirlwall M. (2011) Dissolution methods
693 for strontium isotope stratigraphy: Guidelines for the use of bulk carbonate and
694 phosphorite rocks. *Chemical Geology* **290**, 133-144.

695 Li Y., Li C. and Guo J. (2020) Re-evaluation and optimisation of dissolution methods
696 for strontium isotope stratigraphy based on chemical leaching of carbonate
697 certificated reference materials. *Microchemical Journal* **154**.

698 Liu C., Wang Z. and Raub T. D. (2013) Geochemical constraints on the origin of
699 Marinoan cap dolostones from Nuccaleena Formation, South Australia.
700 *Chemical Geology* **351**, 95–104.

701 Liu C., Wang Z., Raub T. D., Macdonald F. A. and Evans D. A. D. (2014)
702 Neoproterozoic cap-dolostone deposition in stratified glacial meltwater plume.
703 *Earth and Planetary Science Letters* **404**, 22–32.

704 Mazzullo S. J. (1992) Geochemical and neomorphic alteration of dolomite: A review.
705 *Carbonates and Evaporites* **7**.

706 McArthur J. M. (1994) Recent trends in strontium isotope stratigraphy. *Terra Nova*.

707 McArthur J. M., Howarth R. J. and Shields G. A. (2012) Strontium Isotope
708 Stratigraphy, in: Gradstein, F. M., Ogg, J. G., Schmitz, M. B., Ogg, G. M. (Eds.),
709 The geologic time scale 2012. *Elsevier*, pp. 127–144.

710 McArthur J. M., Howarth R. J., Shields G. A. and Zhou Y. (2020) Strontium Isotope
711 Stratigraphy, in: Gradstein, F. M., Ogg, J. G., Schmitz, M. B., Ogg, G. M. (Eds.),
712 The geologic time scale 2020. *Elsevier*, pp. 211-238.

713 McCulloch M. T. (1994) Primitive $^{87}\text{Sr}/^{86}\text{Sr}$ from an Archean barite and conjecture
714 on the Earth's age and origin. *Earth and Planetary Science Letters* **126**, 1–13.

715 Melezhik V. A., Gorokhov I. M., Fallick A. E. and Gjelle S. (2001) Strontium and
716 carbon isotope geochemistry applied to dating of carbonate sedimentation: An
717 example from high-grade rocks of the Norwegian Caledonides. *Precambrian*
718 *Research* **108**, 267-292.

719 Meyer A. C. S., Grundle D. and Cullen J. T. (2021) Selective uptake of rare earth
720 elements in marine systems as an indicator of and control on aerobic bacterial
721 methanotrophy. *Earth and Planetary Science Letters* **558**.

722 Miller N., Johnson P. R. and Stern R. J. (2008) Marine versus non-marine
723 environments for the Jibalah Group, NW Arabian shield: A sedimentologic and
724 geochemical survey and report of possible metazoa in the Dhaiqa formation.
725 *Arabian Journal for Science and Engineering* **33**, 55-77.

726 Moldoveanu G. A. and Papangelakis V. G. (2013) Recovery of rare earth elements
727 adsorbed on clay minerals: II. Leaching with ammonium sulfate.
728 *Hydrometallurgy* **131–132**, 158-166.

729 Montañez I. P., Banner J. L., Osleger D. A., Borg L. E. and Bosserman P. J. (1996)
730 Integrated Sr isotope variations and sea-level history of middle to Upper

731 Cambrian platform carbonates: Implications for the evolution of Cambrian
732 seawater $87\text{Sr}/86\text{Sr}$. *Geology* **24**, 917.

733 Morton J. P. (1985) Rb-Sr dating of diagenesis and source age of clays in Upper
734 Devonian black shales of Texas. *Geological Society of America Bulletin* **96**.

735 Nothdurft L. D., Webb G. E. and Kamber B. S. (2004) Rare earth element
736 geochemistry of Late Devonian reefal carbonates, Canning Basin, Western
737 Australia: Confirmation of a seawater REE proxy in ancient limestones.
738 *Geochimica et Cosmochimica Acta* **68**.

739 Nozaki Y., Zhang J. and Amakawa H. (1997) The fractionation between Y and Ho in
740 the marine environment. *Earth and Planetary Science Letters* **148**.

741 Pogge Von Strandmann P. A. E., Jenkyns H. C. and Woodfine R. G. (2013) Lithium
742 isotope evidence for enhanced weathering during Oceanic Anoxic Event 2.
743 *Nature Geoscience* **6**, 668-672.

744 Pourmand A., Dauphas N. and Ireland T. J. (2012) A novel extraction
745 chromatography and MC-ICP-MS technique for rapid analysis of REE, Sc and
746 Y: Revising CI-chondrite and Post-Archean Australian Shale (PAAS)
747 abundances. *Chemical Geology* **291**, 38-54.

748 Ray J. S., Veizer J. and Davis W. J. (2003) C, O, Sr and Pb isotope systematics of
749 carbonate sequences of the Vindhyan Supergroup, India: Age, diagenesis,
750 correlations and implications for global events. *Precambrian Research* **121**, 103–
751 140.

752 Renwei L., Jenshi C., Shukun Z. and Zhimig C. (2003) Secular variations in carbon
753 isotopic compositions of carbonates from Proterozoic successions in the Ming
754 Tombs Section of the North China Platform. *Journal of Asian Earth Sciences* **22**,
755 329-341.

756 Roerdink D. L., Ronen Y., Strauss H. and Mason P. R. D. (2022) Emergence of felsic
757 crust and subaerial weathering recorded in Palaeoarchean barite. *Nature*
758 *Geoscience* **15**, 227–232.

759 Rutten A. and de Lange G. J. (2002) A novel selective extraction of barite, and its
760 application to eastern Mediterranean sediments. *Earth and Planetary Science*
761 *Letters* **198**, 1-2.

762 Satkoski A. M., Fralick P., Beard B. L. and Johnson C. M. (2017) Initiation of
763 modern-style plate tectonics recorded in Mesoarchean marine chemical
764 sediments. *Geochimica et Cosmochimica Acta* **209**, 216–232.

765 Satkoski A. M., Lowe D. R., Beard B. L., Coleman M. L. and Johnson C. M. (2016)
766 A high continental weathering flux into Paleoproterozoic seawater revealed by
767 strontium isotope analysis of 3.26 Ga barite. *Earth and Planetary Science Letters*
768 **454**, 28–35.

769 Shields G. A. (2007) A normalised seawater strontium isotope curve: possible
770 implications for Neoproterozoic-Cambrian weathering rates and the further
771 oxygenation of the Earth. *eEarth* **2**, 35-42.

772 Shields G. and Veizer J. (2002) Precambrian marine carbonate isotope database:
773 Version 1.1. *Geochemistry, Geophysics, Geosystems* **3**.

774 Spooner E. T. C. (1976) The strontium isotopic composition of seawater, and
775 seawater-oceanic crust interaction. *Earth and Planetary Science Letters* **31**, 167-
776 174.

777 Stammeier J. A., Nebel O., Hippler D. and Dietzel M. (2020) A coherent method for
778 combined stable magnesium and radiogenic strontium isotope analyses in
779 carbonates (with application to geological reference materials SARM 40, SARM
780 43, SRM 88A, SRM 1B). *MethodsX* **7**.

781 Stüeken E. E., Bellefroid E. J., Prave A., Asael D., Planavsky N. J. and Lyons T. W.
782 (2017) Not so non-marine? Revisiting the Stoer Group and the Mesoproterozoic
783 biosphere. *Geochemical Perspectives Letters* **3**.

784 Tan C., Lu Y., Li X., Song H., Lv D., Ma X., Fan R. and Deng S. (2020) Carbon,
785 oxygen and strontium isotopes of the Mesoproterozoic Jixian System (1.6-1.4
786 Ga) in the southern margin of the North China Craton and the geological
787 implications. *International Geology Review* **00**, 1–18.

788 Taylor S. R. and McLennan S. M. (1981) The rare earth element evidence in
789 precambrian sedimentary rocks: Implications for crustal evolution. *Developments*
790 *in Precambrian Geology* **4**.

791 Tessier A., Campbell P. G. C. and Bisson M. (1979) Sequential Extraction Procedure
792 for the Speciation of Particulate Trace Metals. *Analytical Chemistry* **51**.

793 Tostevin R., Shields G. A., Tarbuck G. M., He T., Clarkson M. O. and Wood R. A.
794 (2016) Effective use of cerium anomalies as a redox proxy in carbonate-
795 dominated marine settings. *Chemical Geology* **438**, 146–162.

796 Vahrenkamp V. C. and Swart P. K. (1990) New distribution coefficient for the
797 incorporation of strontium into dolomite and its implications for the formation of
798 ancient dolomites. *Geology* **18**.

799 Veizer J. (1989) Strontium isotopes in seawater through time. *Annual review of earth*
800 *and planetary sciences* **17**, 141-167.

801 Veizer J., Ala D., Azmy K., Bruckschen P., Buhl D., Bruhn F., Garden G. A. F.,
802 Diener A., Ebneith S., Godderis Y., Jasper T., Korte C., Pawellek F., Podlaha O.
803 G. and Strauss H. (1999) $^{87}\text{Sr}/^{86}\text{Sr}$, $\delta^{13}\text{C}$ and $\delta^{18}\text{O}$ evolution of Phanerozoic
804 seawater. *Chemical Geology* **161**, 59-88.

805 Verdel C., Phelps B. and Welsh K. (2018) Rare earth element and $^{87}\text{Sr}/^{86}\text{Sr}$ step-
806 leaching geochemistry of central Australian Neoproterozoic carbonate.
807 *Precambrian Research* **310**.

808 Webb G. E. and Kamber B. S. (2000) Rare earth elements in Holocene reefal
809 microbialites: A new shallow seawater proxy. *Geochimica et Cosmochimica*
810 *Acta* **64**.

811 Wierzbowski H., Anczkiewicz R., Bazarnik J. and Pawlak J. (2012) Strontium isotope
812 variations in Middle Jurassic (Late Bajocian-Callovian) seawater: Implications
813 for Earth's tectonic activity and marine environments. *Chemical Geology* **334**,
814 171-181.

815 Zhang K. and Shields G. A. (2022) Sedimentary Ce anomalies: Secular change and
816 implications for paleoenvironmental evolution. *Earth-Science Reviews* **229**,
817 104015.

818 Zhang K., Zhu X. K. and Yan B. (2015) A refined dissolution method for rare earth
819 element studies of bulk carbonate rocks. *Chemical Geology* **412**.

820 Zhang K., Zhu X., Wood R. A., Shi Y., Gao Z. and Poulton S. W. (2018)
821 Oxygenation of the Mesoproterozoic ocean and the evolution of complex
822 eukaryotes. *Nature Geoscience* **11**, 345–350.

823 Zhong S. and Mucci A. (1995) Partitioning of rare earth elements (REEs) between
824 calcite and seawater solutions at 25°C and 1 atm, and high dissolved REE
825 concentrations. *Geochimica et Cosmochimica Acta* **59**.

826 Zhou Y., von Strandmann P. A. E. P., Zhu M., Ling H., Manning C., Li D., He T. and
827 Shields G. A. (2020) Reconstructing tonian seawater $^{87}\text{Sr}/^{86}\text{Sr}$ using calcite
828 microspar. *Geology* **48**, 462–467.

829